Research Paper

Combination of bulk RNA sequencing and scRNA sequencing uncover the molecular characteristics of MAPK signaling in kidney renal clear cell carcinoma

Xiunan Li[1,*], Hewen Guan[2,*], Chuanyu Ma[1,*], Yunfei Dai[3], Ji Su[4], Xu Chen[3], Qihang Yuan[3], Jianbo Wang[1]

[1]Department of Urology, The First Affiliated Hospital of Dalian Medical University, Dalian, Liaoning, China
[2]Department of Dermatology, First Affiliated Hospital of Dalian Medical University, Dalian, Liaoning, China
[3]Department of General Surgery, First Affiliated Hospital of Dalian Medical University, Dalian, Liaoning, China
[4]Department of Urology, Central Hospital of Benxi, Benxi, Liaoning, China
*Equal contribution

Correspondence to: Jianbo Wang, Qihang Yuan, Xu Chen; **email:** wangjianbo@dmu.edu.cn; qihangdy@163.com, https://orcid.org/0000-0001-7516-7620; chenxdy@163.com, https://orcid.org/0000-0001-9681-1630

ABSTRACT

The MAPK signaling pathway significantly impacts cancer progression and resistance; however, its functions remain incompletely assessed across various cancers, particularly in kidney renal clear cell carcinoma (KIRC). Therefore, there is an urgent need for comprehensive pan-cancer investigations of MAPK signaling, particularly within the context of KIRC. In this research, we obtained TCGA pan-cancer multi-omics data and conducted a comprehensive analysis of the genomic and transcriptomic characteristics of the MAPK signaling pathway. For in-depth investigation in KIRC, status of MAPK pathway was quantitatively estimated by ssGSEA and Ward algorithm was utilized for cluster analysis. Molecular characteristics and clinical prognoses of KIRC patients with distinct MAPK activities were comprehensively explored using a series of bioinformatics algorithms. Subsequently, a combination of LASSO and COX regression analyses were utilized sequentially to construct a MAPK-related signature to help identify the risk level of each sample. Patients in the C1 subtype exhibited relatively higher levels of MAPK signaling activity, which were associated with abundant immune cell infiltration and favorable clinical outcomes. Single-cell RNA sequencing (scRNA-seq) analysis of KIRC samples identified seven distinct cell types, and endothelial cells in tumor tissues had obviously higher MAPK scores than normal tissues. The immunohistochemistry results indicated the reduced expression levels of PAPSS1, MAP3K11, and SPRED1 in KIRC samples. In conclusion, our study represents the first integration of bulk RNA sequencing and single-cell RNA sequencing to elucidate the molecular characteristics of MAPK signaling in KIRC, providing a solid foundation for precision oncology.

INTRODUCTION

Originating from renal tubular epithelial cells, renal cell carcinoma is a malignant tumor accounts for nearly 80% of renal malignancies [1]. Kidney renal clear cell carcinoma (KIRC), with rising incidence and dismal prognosis, is the most common type of renal cell carcinoma [2]. Unfortunately, KIRC is intrinsically resistant to radiation and chemotherapy and only a limited number of treatments such as targeted therapy can be taken [3]. It is not only urgent but also necessary to explore sensitive biomarkers and treatment options for KIRC patients to improve the prognosis.

The mitogen-activated protein kinase (MAPK) signaling pathway is significant in inter- and intra-cellular communication, which affects the cellular processes such as cell proliferation and differentiation [4]. Through three capital kinases: mitogen-activated protein kinase (MAPK), mitogen-activated protein kinase kinase, and mitogen-activated protein kinase kinase kinase, MAPK pathway transforms external stimuli into cellular responses [5]. Current studies concentrating on the influence of the MAPK pathway on the development and metastasis of cancer indicate that the signaling pathway actually acts as a regulator in many cancers such as colorectal cancer and non-small cell lung cancer [5–8]. In addition, MAPK signaling was identified as a potential mechanism to regulate and tumor resistance and drug sensitivity [9].

However, few in-depth researches are reported to reveal the influence of MAPK pathway in KIRC and other cancers. In this research, the roles of MAPK pathway in pan-cancer are summarized and the relation between MAPK pathway and KIRC is purposefully explored. First, 3 different KIRC subtypes with different MAPK signaling activity were identified. Subsequently, the influences of MAPK signaling on the metabolism-related pathways, immune-related pathways, immune response, and ICG expression were investigated. Then 11 hub genes (i.e., SPRED3, ACTB, ARAF, MAP3K11, PAPSS1, TLN1, CALM1, AGK, MAP2K2, MAPK1, SPRED1), selected from all the MAPK-related genes, were utilized to construct a prognostic signature. The signature helped to distinguish KIRC samples with different risk levels. Endothelial cells in tumor tissues had obviously higher MAPK scores than normal tissues. The immunohistochemistry indicated that the PAPSS1, MAP3K11, and SPRED1 showed lower IHC score in KIRC compared with para-cancer samples. All the discrepancies between high- and low-risk subgroups were explored and all these could be potential therapy targets in KIRC.

MATERIALS AND METHODS

Data acquisition

In the current study, the pan-cancer mRNA expression, single nucleotide variation (SNV), copy number variation (CNV), DNA methylation data were obtained from The Cancer Genome Atlas (TCGA) database (https://portal.gdc.cancer.gov/). In addition, the clinical parameters of KIRC were downloaded simultaneously. The KIRC transcriptome profiles were also searched in the ArrayExpress database (https://www.ebi.ac.uk/arrayexpress/). The Molecular Signatures Database (MSigDB) were searched

to obtain the MAPK pathway and other signaling pathways (https://www.gsea-msigdb.org/gsea/msigdb/human/geneset/REACTOME_ONCOGENIC_MAPK_SIGNALING.html?keywords=REACTOME_ONCOGENIC_MAPK_SIGNALING). Immune checkpoint genes (ICGs) were summarized according to the review [10].

Comprehensive assessment of MAPK pathway in pan-cancer

Recent studies indicated that MAPK pathway affect the biological behavior and prognosis of malignancies and targeting MAPK pathway may be a novel perspective for cancer therapy [9, 11–14]. Nonetheless, the prognostic value, expression level, CNV, SNV and methylation of key genes in MAPK pathway in pan-cancer are reported dispersedly and sparsely. Subsequently, comprehensive assessments of genes regulating MAPK pathway were conducted in pan-cancer. First, the expression of MAPK genes in each cancer were compared with those in corresponding normal tissues and each fold change was calculated respectively [15]. Then the CNV gain, CNV loss, and SNV were summarized and presented utilizing heatmap. In addition, the estimations of DNA methylation of MAPK genes in pan-cancer were conducted by comparing with corresponding normal samples [16].

MAPK-based cluster analysis in KIRC

Due to the potential role of MAPK signaling pathway in KIRC, the activation of the pathway was assessed for the first step. With the expression levels of the MAPK genes in KIRC, the status of MAPK pathway was quantitatively estimated by ssGSEA. After acquiring the MAPK score, KIRC samples were grouped into cluster1 with MAPK-active status, cluster2 with MAPK-normal status, and cluster3 with MAPK-inactive status through cluster analysis by Ward algorithm. Then the violin plots of MAPK scores were constructed and the survival curves were plotted to explore the survival discrepancies among these three clusters. Following a methodology similar to previous studies [17, 18], we curated a selection of classical immune pathways, metabolic pathways, and cell death pathways. Initially, we computed pathway scores using the "gsva" package, providing a measure of each pathway's activity. Subsequently, we consolidated these scores and visually represented them in a heatmap format. Statistical analyses were carried out using the "kruskal.test" function in R.

For investigation of the tumor microenvironment (TME) in the three clusters, the "ESTIMATE" package in R and various immune-related algorithms including TIMER, QUANTISEQ, MCPCOUNTER, XCELL,

EPIC, and CIBERSORT were utilized for further analyses [19]. Additionally, the expression levels of common immune checkpoint genes were compared in the three clusters utilizing Kruskal-Wallis test. By applying the ssGSEA, the immune response was estimated. Next, we delved into the correlations between MAPK signaling and the infiltration of immune cells, and the findings were visually presented in a heatmap.

For further exploration about the discrepancies of the drug sensitivity in the three clusters, the Genomics of Drug Sensitivity in Cancer database (GDSC; https://www.cancerRxgene.org) was utilized to predict therapy response. The GDSC database linked drug sensitivity to genomic data then the IC50 of the samples were obtained. Of note, a lower IC50 suggests that the cancer cells are more sensitive to the compound.

Construction and validation of a MAPK-related signature

In view of the significant role of MAPK pathway in KIRC, then all the MAPK genes were utilized to construct a signature to help distinguish KIRC samples. To ensure adequate validation, all samples in TCGA were randomly divided into a training set and a test set 1 at a nearly 1:1 ratio. In addition, all samples from TCGA and ArrayExpress were defined as test2 cohort and test3 cohort, respectively.

In train cohort, LASSO and Cox regression analysis were utilized to identify the hub genes and construct a MAPK-related signature (MAPKS) to help distinguish KIRC samples. After identifying the MAPKS, the "predict" function in R was utilized to calculate the risk score. Then all the samples were grouped into high- and low-risk subgroups based on the median risk score in train cohort. In the four cohorts, the following discrepancies between high- and low-risk subgroups were investigated for comprehensive validation: (1) the survival analysis was performed to identify the survival discrepancy; (2) the receiver-operating characteristic (ROC) curves were utilized to determine the diagnostic value of MAPKS; (3) "ESTIMATE" package in R was utilized to assess the tumor microenvironment [20]; (4) TIMER, QUANTISEQ, and many other algorithms introduced above were utilized to assess the immune response in the TME [21]; (5) the expression levels of ICGs in high- and low-risk subgroups were compared.

The estimation of MAPK pathway and gene expression of MAPKS genes on the basis of scRNA-seq data

KIRC scRNA-seq data, GSE159115, was obtained from the GEO database. The scRNA-seq data of KIRC

were analyzed based on the standard protocols of Seurat [22]. Those cells with less than 200 or more than 7000 count features were removed. In addition, cells with mitochondrial RNA percentage > 10 were also excluded. Then the data were normalized, scaled and processed for PCA analysis. The Harmony package was utilized to remove the batch effect. The "FindClusters" function was used to cluster cells at an appropriate resolution. The t-SNE was utilized to visualize the data. Based on the typical cell-type markers, all the subpopulations were annotated. The activity of MAPK pathway was estimated utilizing five well-known algorithms (i.e. AUCell, UCell, singscore, Add, and GSVA). Of note, the scores from the five algorithms mentioned above were summed to obtain a total score, which we referred to as "Scoring". We employed the "wilcox.test" to compare pathway activities between KIRC and normal samples at the single-cell resolution.

Identification of hub genes in the occurrence of KIRC

On the basis of the genes in the MAPKS, in-depth exploration was conducted to identify hub genes in KIRC. First, the GEPIA online server was utilized to compare the mRNA expression of all the module genes in our signature. Then the relationship between the expression of each gene and tumor stage in KIRC was explored. In addition, the Biomarker Exploration for Solid Tumors (BEST) web server was used for further investigation of the relationship between the expression of each gene and tumor grade.

External validation of hub genes in MAPKS based on the tissue microarray and immunohistochemistry (IHC)

Human KIRC tissue chips were purchased from Zhuoli Biotechnology Co., Shanghai, China. First, EDTA was used to extract antigens after tissue dewaxing. After placing with the primary antibodies, the tissue sections were incubated with the secondary antibodies. Then the diaminoaniline staining was made and hematoxylin was utilized to re-stain. Finally, the IHC morphology of 80 KIRC samples and 80 normal samples were completed. The IHC scores were analyzed by two independent pathologists based on the staining intensity and the percentage of positive-stained cells intensity.

Availability of data and materials

The datasets analyzed in this work may be found in the Supplementary Materials or contact with the corresponding author.

RESULTS

Changes of mRNA expression, CNV, SNV, and methylation of MAPK-related genes in pan-cancer

First, the expression levels of MAPK-related genes were summarized in pan-cancer. It was shown in Figure 1A that obvious up-regulation of ESRP1 existed in CESC, perceptible up-regulation of DUSP9 existed in LUSC, while significant down-regulation of DUSP9 existed in KIRC and KIRP. As a major influence in the gene expression levels, the CNV gain and CNV loss needed to be paid more attention to. As shown in Figure 1B, the pinker the color, the higher the CNV gain frequency. In KICH, the number of MAPK genes with high CNV gain frequency is maximum. And in KIRC, CAMK2A and FAM114A2 had obviously high CNV gain frequency. As for the CNV loss frequency in the Figure 1C, the number of MAPK genes with high CNV loss frequency is also maximum in KICH. And in KIRC, ATG7, RAF1, and TRAK1 had high CNV loss frequency. In addition, increasing SNV frequency of KRAS existed in COAD, LUAD, PAAD, READ, and UCEC (Figure 1D). As for the DNA methylation, the cancers and the corresponding genes with hyper-methylation were as follows: BRCA: VWF and ITGB3; COAD: QKI, DUSP9, and CNKSR2; KIRC: CNKSR1; PRAD: VWF, LMNA, and ITGB3; UCEC: ITGB3 and APBBAIP (Figure 1E).

MAPK-based cluster analysis in KIRC

For further demonstration of the role of MAPK pathway in KIRC, all KIRC samples were classified into three clusters (Figure 2A). Subsequently, the MAPK scores in these three clusters were compared and the violin plots in Figure 2B indicated that the cluster1 was MAPK-active cluster, cluster2 was the MAPK-normal cluster while C3 was the MAPK-inactive cluster (Enrichment score: C1>C2>C3, p<0.01). The survival analysis indicated that the prognosis of cluster 1 was better than that of cluster 2 and the prognosis of cluster 3 was worse than that of cluster 2. All the discrepancies of the survival rate in the three clusters were statistical (Figure 2C).

MAPK-based discrepancies in signaling activity and cell death status

With different activity of MAPK signaling, these three clusters had different metabolism signaling, immune signaling. All the statistical discrepancies were exhibited in the form of heatmap. As is shown in Figure 2D, most metabolism signaling had decreasing activity in C2, but AMINO_SUGAR_AND_NUCLEOTIDE_SUGAR_ METABOLISM, CYSTEINE_AND_METHIONINE_ METABOLISM, and SULFUR_METABOLISM had

decreasing activity in C1 and INOSITOL_PHOSPHATE_ METABOLISM had decreasing activity in C3. The discrepancies of immune signaling shown in Figure 2E indicated that most immune pathways had decreasing activity in C3 except BASE_EXCISION_REPAIR and PROTEASOME. As for the cell death status shown in Figure 2F, it was indicated that all the types of cell death (i.e., curroptosis, immunogenic cell death, necroptosis, apoptosis, autophagy, ferropotosis, phagocytosis, necrosis, pyroptosis, PANoptosis, disulfidptosis) had decreasing activation in C3.

MAPK-based discrepancies in immune microenvironment

As is known, immune cells are primary components in TME. With various algorithms including TIMER, QUANTISEQ, MCPCOUNTER, XCELL, EPIC, and CIBERSORT, it was found that the infiltration of immune cells differed in the three clusters and most immune cells including B cell, CD4+ T cell, macro-phage, neutrophil, and mast cell had lower proportions in C3 (Figure 3A). Further exploration about the correlations between MAPK genes and immune cell infiltration were shown in a heatmap in Figure 3B. The redder the color, the closer the positive correlation. The bluer the color, the closer the negative correlation. As for the correlation between MAPK score and the infiltration of immune cells, it was found that the infiltration of most immune cells except Tfh had positive correlation with MAPK score (Figure 3C). Of note, the responses of mast cell, Treg, neutrophil, and type-II-IFN-Response are positively related to the MAPK score (R>0.3, p<0.05) (Figure 3D). Additionally, the immune checkpoint genes had different expression levels in the three clusters. The following genes had lowest expression level in C3: TNFSF15, JAK2, PDCD1LG2, LDHA, CD244, CD28, YTHDF1, NRP1, SIGLEC15, ICOS, CD86, CD44, TNFSF4, CD274, CD200R1, HAVCR2, CD276, PVR, LAIR1, CD80, B2M, BTLA, and PTPRC (p<0.05) (Figure 3E).

MAPK-based drug sensitivity analysis in KIRC

Currently, the treatment of advanced KIRC mostly depends on molecular targeted drugs. Till now, many types of targeted drugs including sorafenib and sunitinib have been listed in NCCN for a first- or second-line treatment of metastatic kidney cancer [23]. In view of the significant role of the targeted therapy in KIRC, common targeted drugs were taken into consideration for the exploration of the sensitive drugs. The lower the IC50, the more sensitive the compound. For Irinotecan and Topotecan, samples in cluster1 had lowest IC50. For Cisplatin, Cyclophosphamide, Cytarabine, Docetaxel, Gefitinib, Lapatinib, Nilotinib, Sorafenib,
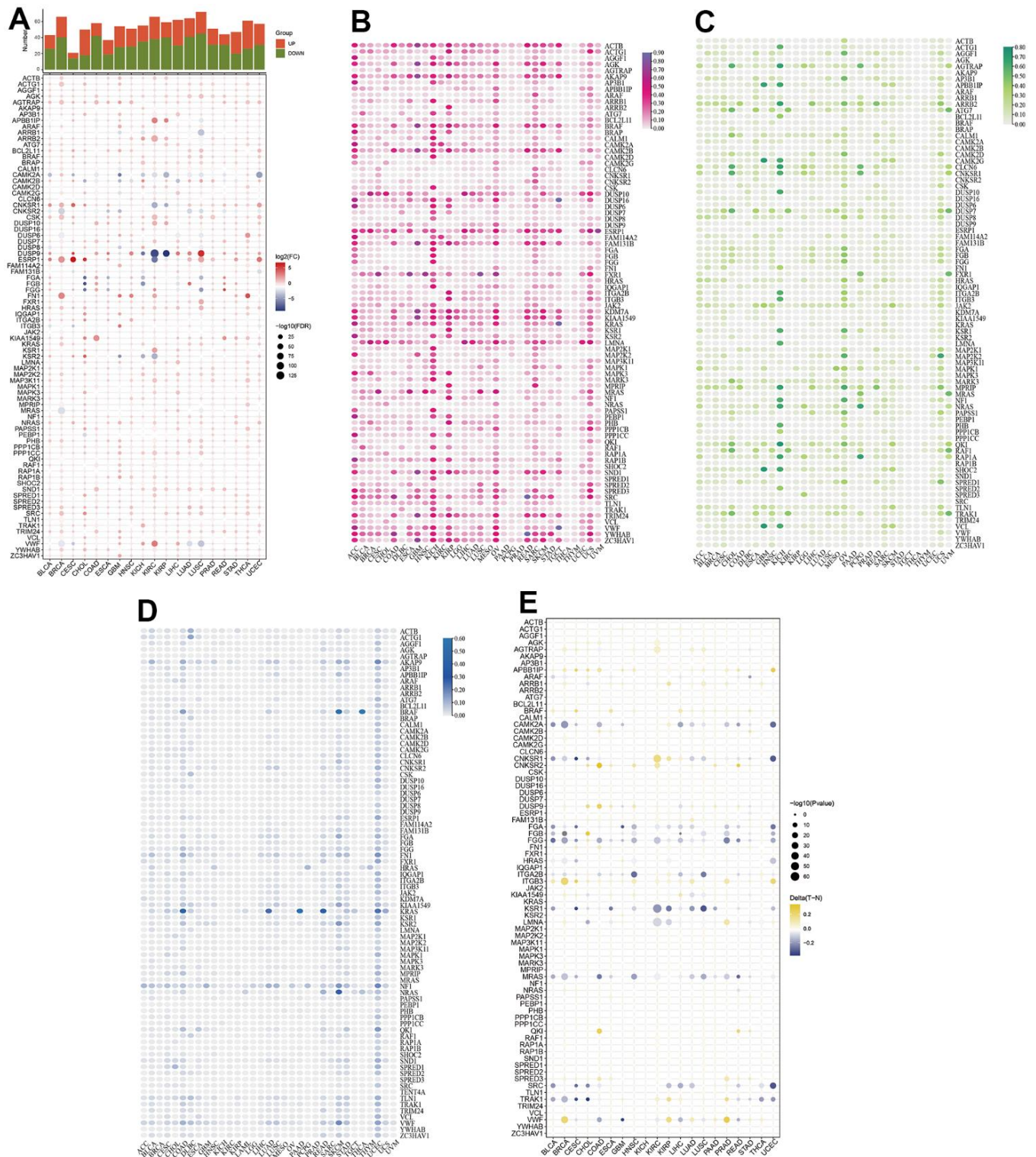
Figure 1. Comprehensive assessment of MAPK pathway in pan-cancer. (**A**) mRNA expression of MAPK-related genes. (**B**) CNV gain of MAPK-related genes. (**C**) CNV loss of MAPK-related genes. (**D**) SNV frequency of MAPK-related genes. (**E**) DNA methylation of MAPK-related genes.

Temozolomide, and Vinblastine, samples in cluster3 had lowest IC50 (Figure 4).

Construction and validation of a MAPK-related signature

Samples in the train cohort were utilized to construct MAPKS. After conducting LASSO regression analysis, univariate Cox regression analysis and multivariate Cox regression analysis, 11 hub genes (i.e., SPRED3, ACTB, ARAF, MAP3K11, PAPSS1, TLN1, CALM1, AGK, MAP2K2, MAPK1, SPRED1) were selected to construct a MAPKS. On the basis of the expression levels of these 11 genes, the risk score of each sample was calculated utilizing the "predict" function in R. Based on the median risk score, samples were divided
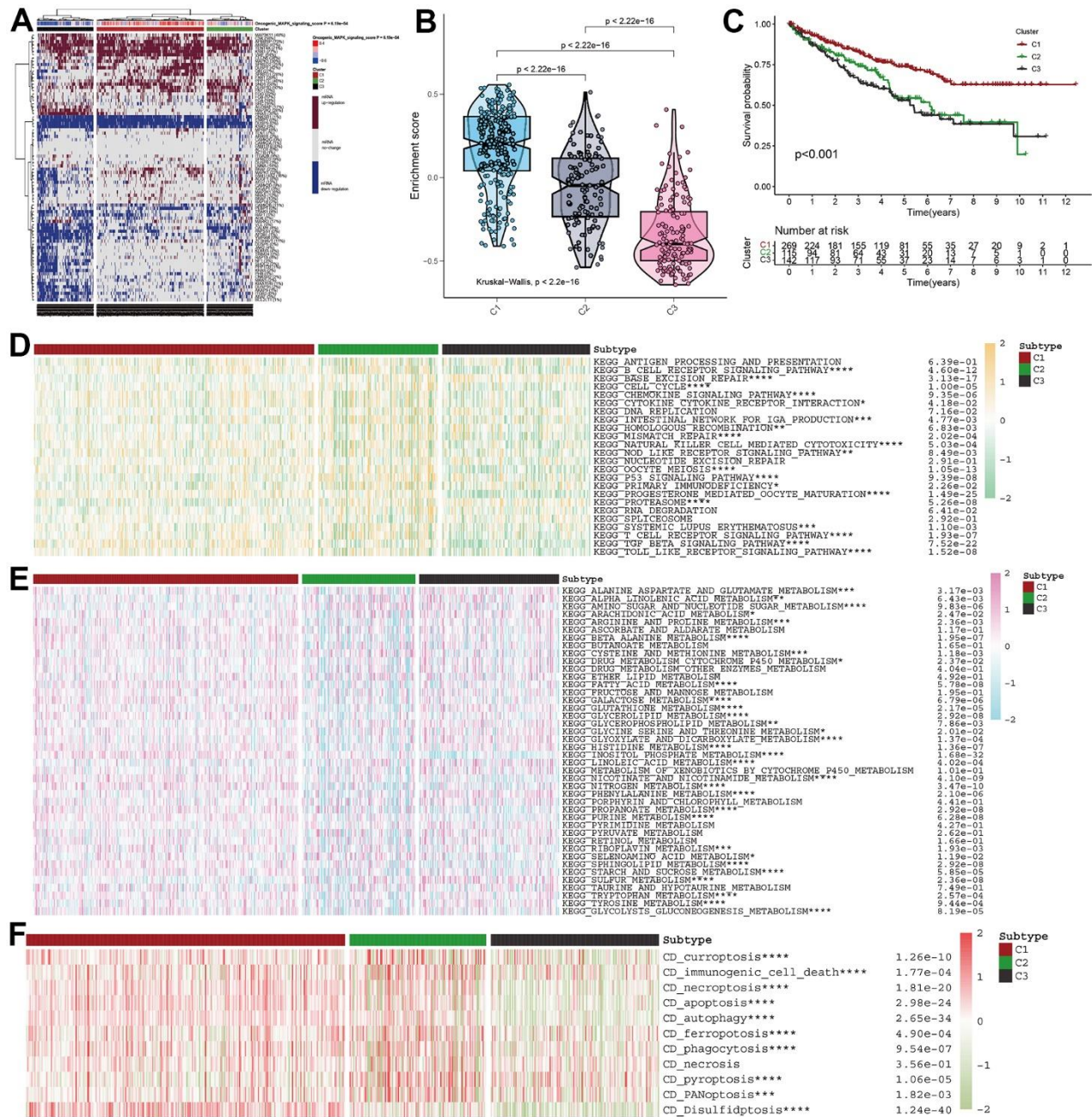
Figure 2. MAPK-based cluster analysis in KIRC. (**A**) Three clusters were obtained and displayed by the heatmap. (**B**) The violin plot showing the enrichment scores of these three clusters. (**C**) The distinct of survival probability in these three clusters. (**D**) The discrepancies of metabolism pathway activity in the three clusters. (**E**) The discrepancies of immune pathway activity in the three clusters. (**F**) The discrepancies of cell death status in the three clusters.
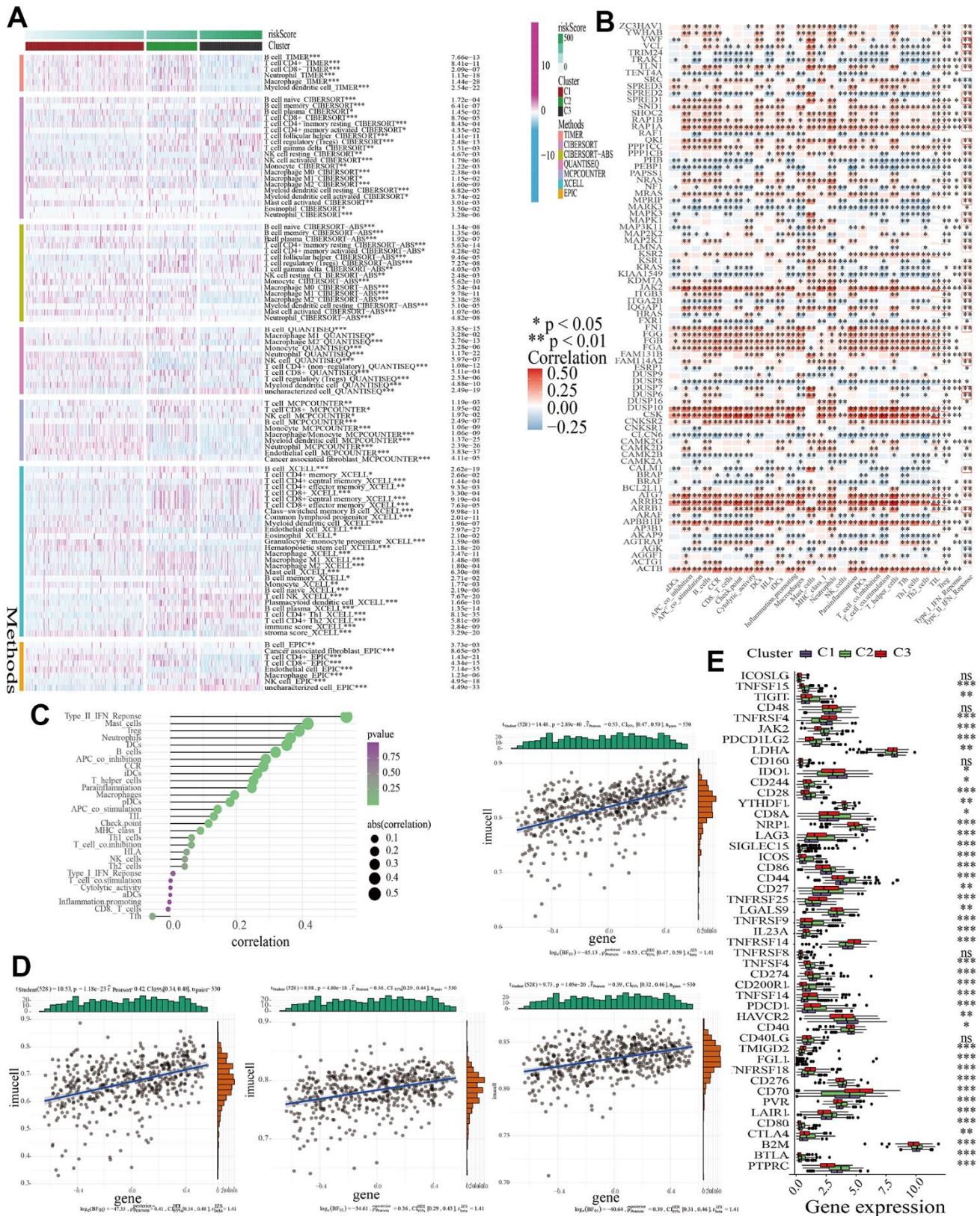
Figure 3. The discrepancies of TME in the three clusters. (**A**) A heatmap showing the infiltration of various immune cells. (**B**) The correlations between the expression of MAPK genes and the infiltration of various immune cells. (**C**) The correlations between MAPK score and the infiltration of various immune cells. (**D**) The correlations between MAPK score and the response of mast cell, Treg, neutrophil, and type-II-IFN-Response. (**E**) The discrepancies of ICG expression in the three clusters.

into high- and low-risk subgroups (Figure 5A). Then the Figure 5B depicted the distributions of the risk score and survival status. Likewise, the survival analysis indicated that patients in high-risk subgroup had lower survival probability (Figure 5C). The AUCs of the ROC curves had values of 0.768, 0.772, and 0.804, respectively, for 1-, 3-, and 5-year survival (Figure 5D). Based on the "ESTIMATE", it was found that samples in high-risk subgroup had higher immune score but lower tumor purity (Figure 5E). As for immune response in the two subgroups, Treg, Tfh, and gamma delta T cell had higher proportion, while Neutrophil and Endothelial cell had lower proportion in high-risk subgroup in train cohort (Figure 5F). The expression of ICGs in the high- and low-risk subgroups also differed from each other. The expression of most ICGs (i.e., CD40LG, TNFRSF25, CD27, CD70, TNFRSF9, CD48, LAG3, PTPRC, TNFRSF4, PDCD1, CD80, CD28, ICOS, IL23A, TIGIT, SIGLEC15) up-regulated while NRP1 and JAK2 down-regulated in the high-risk subgroup (Figure 5G).

For further signature validation, all the analyses conducted above were performed in the test1, test2, and test3 cohorts. In the three test cohorts, similar results were obtained. First, risk scores were calculated and then all the samples were grouped into high- and low-risk subgroups in the three test cohorts respectively (Figures 6A, 7A, 8A). The distributions of the risk scores and survival status were showed in Figures 6B, 7B, 8B. The survival analysis revealed that samples in the high-risk subgroup were more likely to die (Figures 6C, 7C, 8C). The AUCs of the ROC curves also demonstrated the diagnostic value of the MAPKS: the AUCs had values of 0.672, 0.621, and 0.613 in test1 cohort, 0.719, 0.697, and 0.712 in test2 cohort, and 0.909, 0.811, and 0.846 in test3 cohort for 1-, 3-, and 5-year respectively (Figures 6D,7D,8D). Samples in the high-risk subgroup in the three cohorts also showed higher immune score but lower tumor purity (Figures 6E, 7E, 8E). As for the immune response, Treg had higher proportion while Endothelial cell had lower
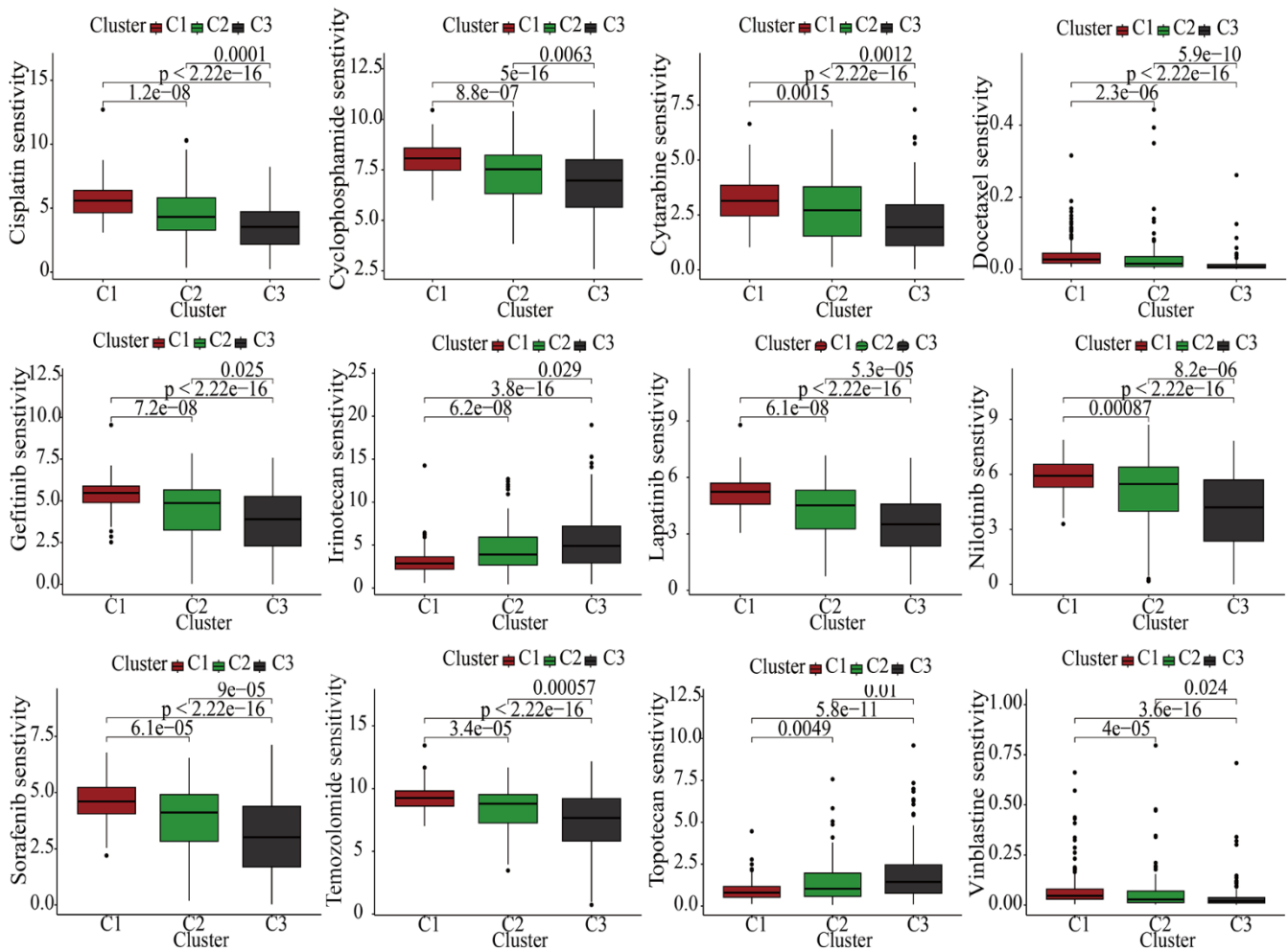

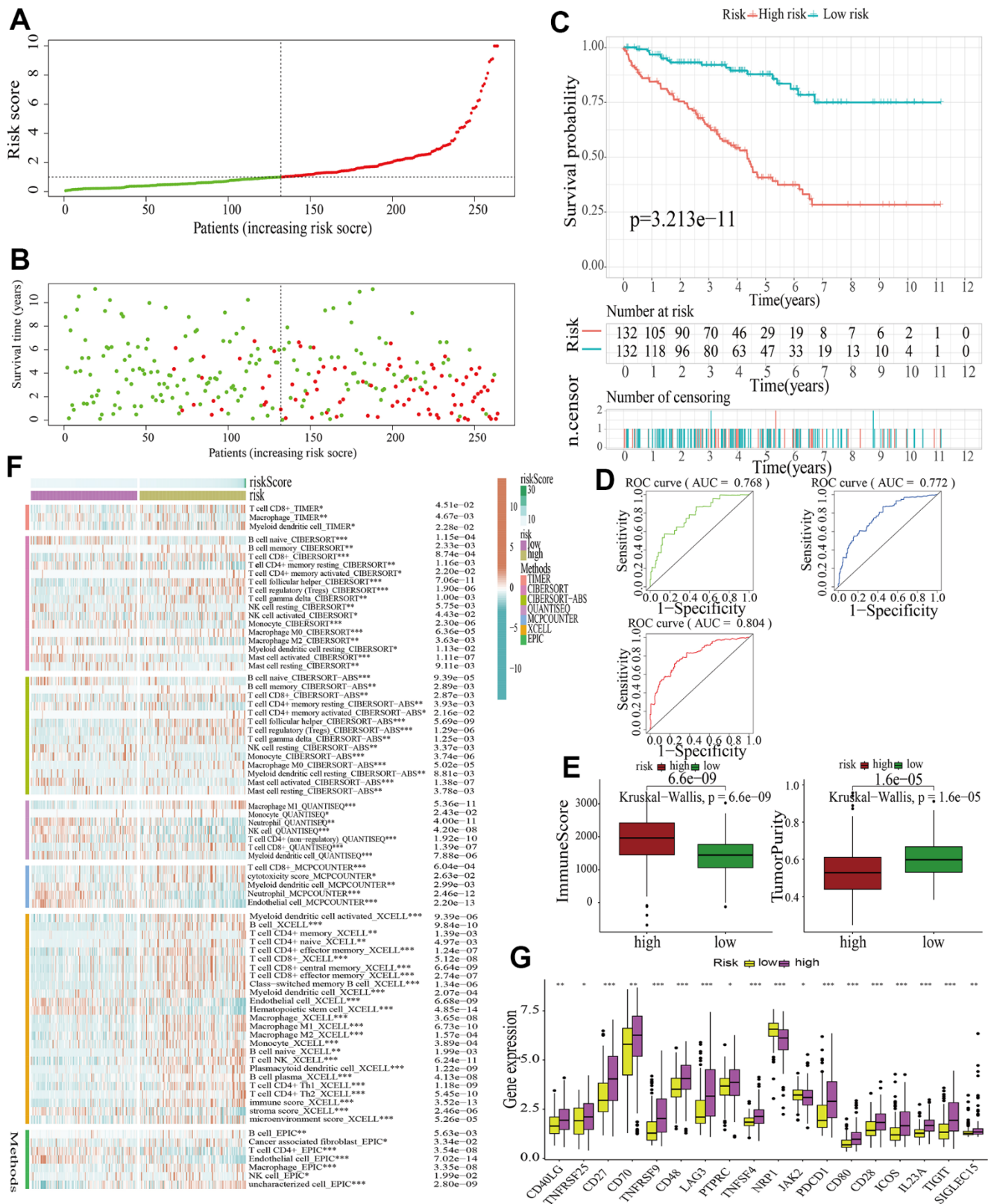Figure 4. The discrepancies of drug sensitivities in the three clusters.

Figure 5. Identification of a MAPK-related signature in train cohort. (**A**) The distinguishment of high- and low-risk subgroups on the basis of the median risk score. (**B**) The distributions of the risk score and survival status. (**C**) Survival analysis in train cohort. (**D**) ROC curves of 1-, 3-, and 5-year survival. (**E**) Assessment of TME by "ESTIMATE". (**F**) The discrepancies of immune response in high- and low-risk subgroups. (**G**) The discrepancies of ICD expression in high- and low-risk subgroups.
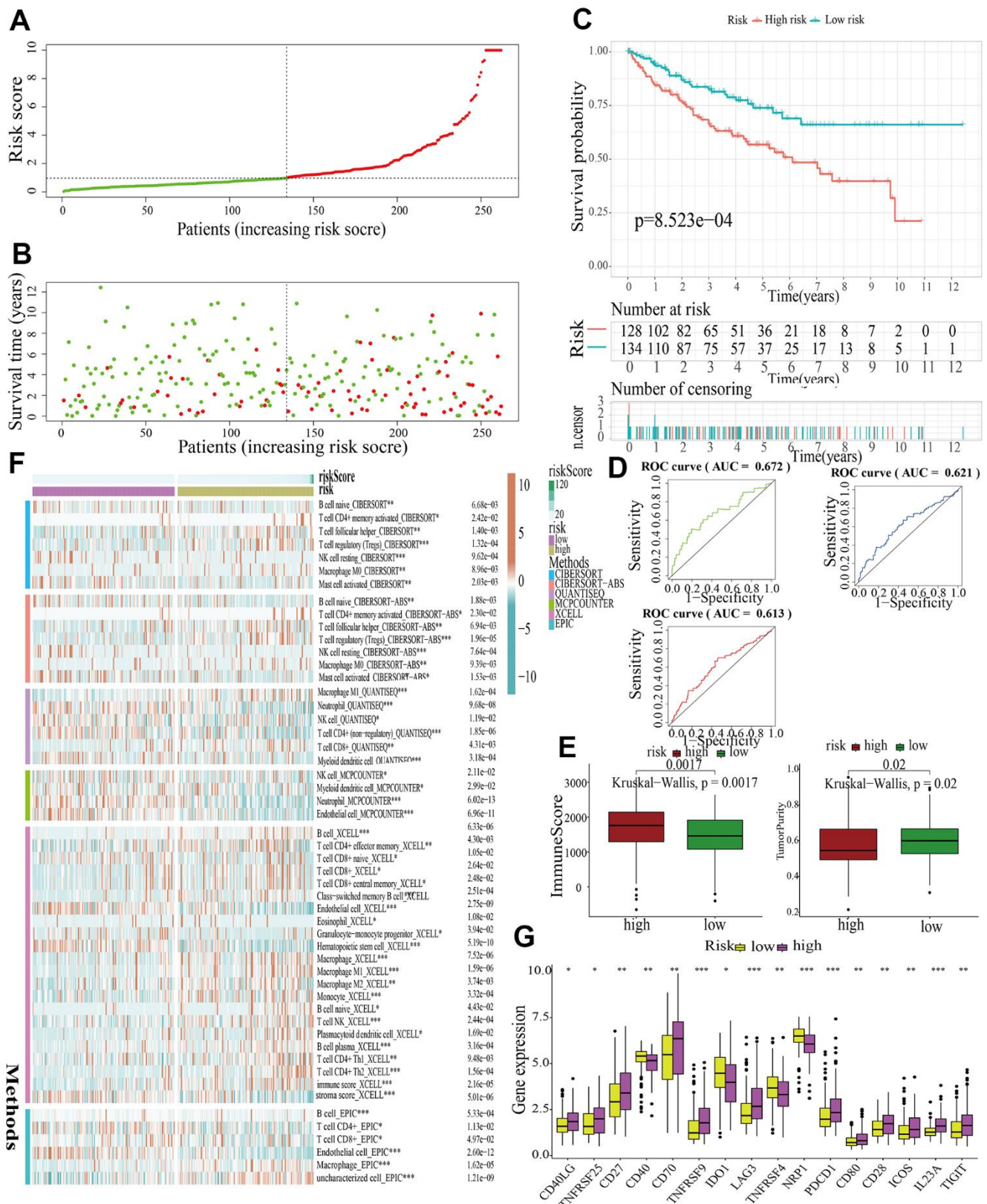
Figure 6. Internal validation of a MAPK-related signature in test1 cohort. (**A**) The distinguishment of high- and low-risk subgroups based on the median risk score in train cohort. (**B**) The distributions of the risk score and survival status. (**C**) Survival analysis in test1 cohort. (**D**) ROC curves of 1-, 3-, and 5-year survival. (**E**) Assessment of TME by "ESTIMATE". (**F**) The discrepancies of immune response in high- and low-risk subgroups. (**G**) The discrepancies of ICD expression in high- and low-risk subgroups.
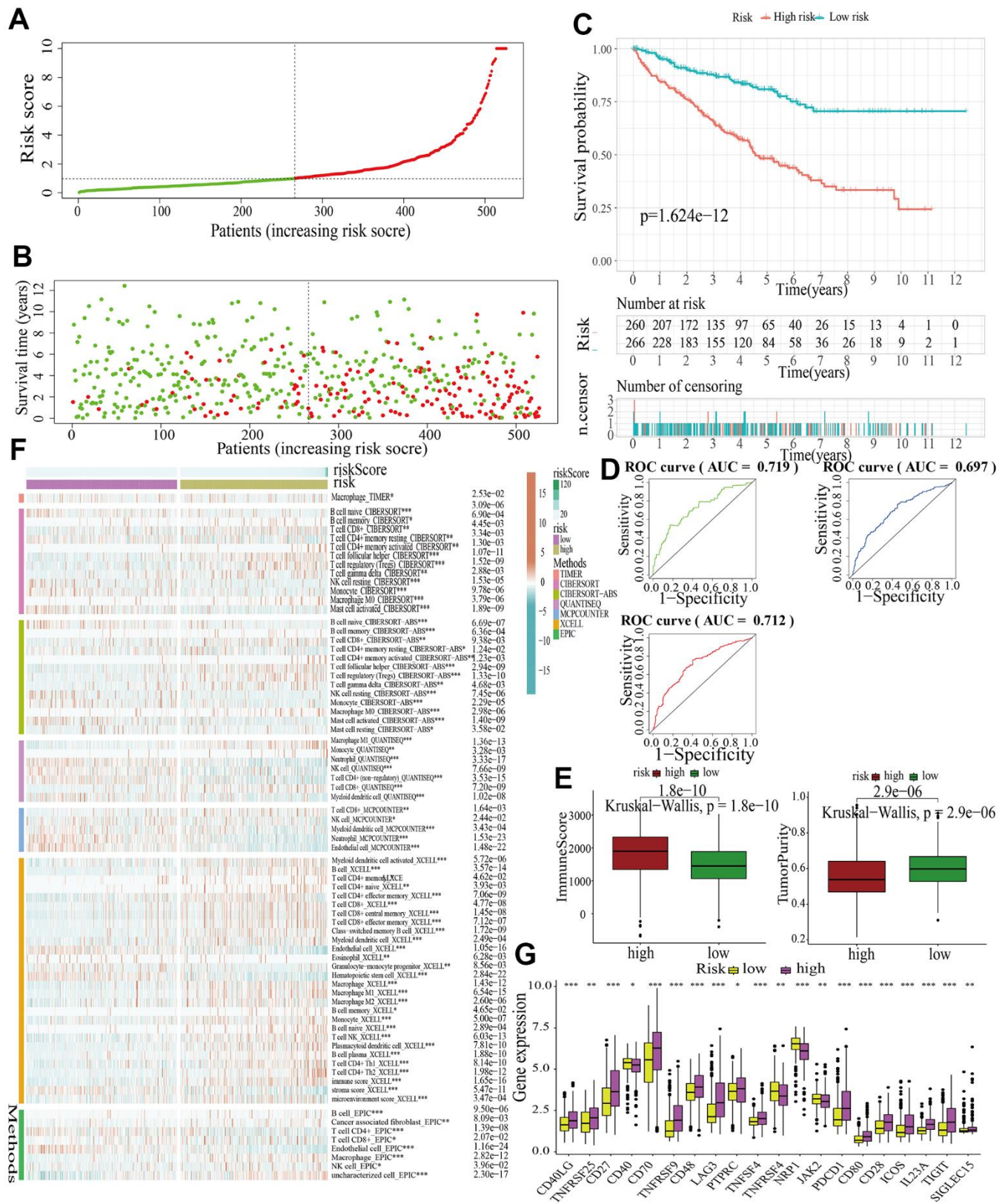
Figure 7. Internal validation of a MAPK-related signature in test2 cohort. (**A**) The distinguishment of high- and low-risk subgroups based on the median risk score in train cohort. (**B**) The distributions of the risk score and survival status. (**C**) Survival analysis in test2 cohort. (**D**) ROC curves of 1-, 3-, and 5-year survival. (**E**) Assessment of TME by "ESTIMATE". (**F**) The discrepancies of immune response in high- and low-risk subgroups. (**G**) The discrepancies of ICD expression in high- and low-risk subgroups.
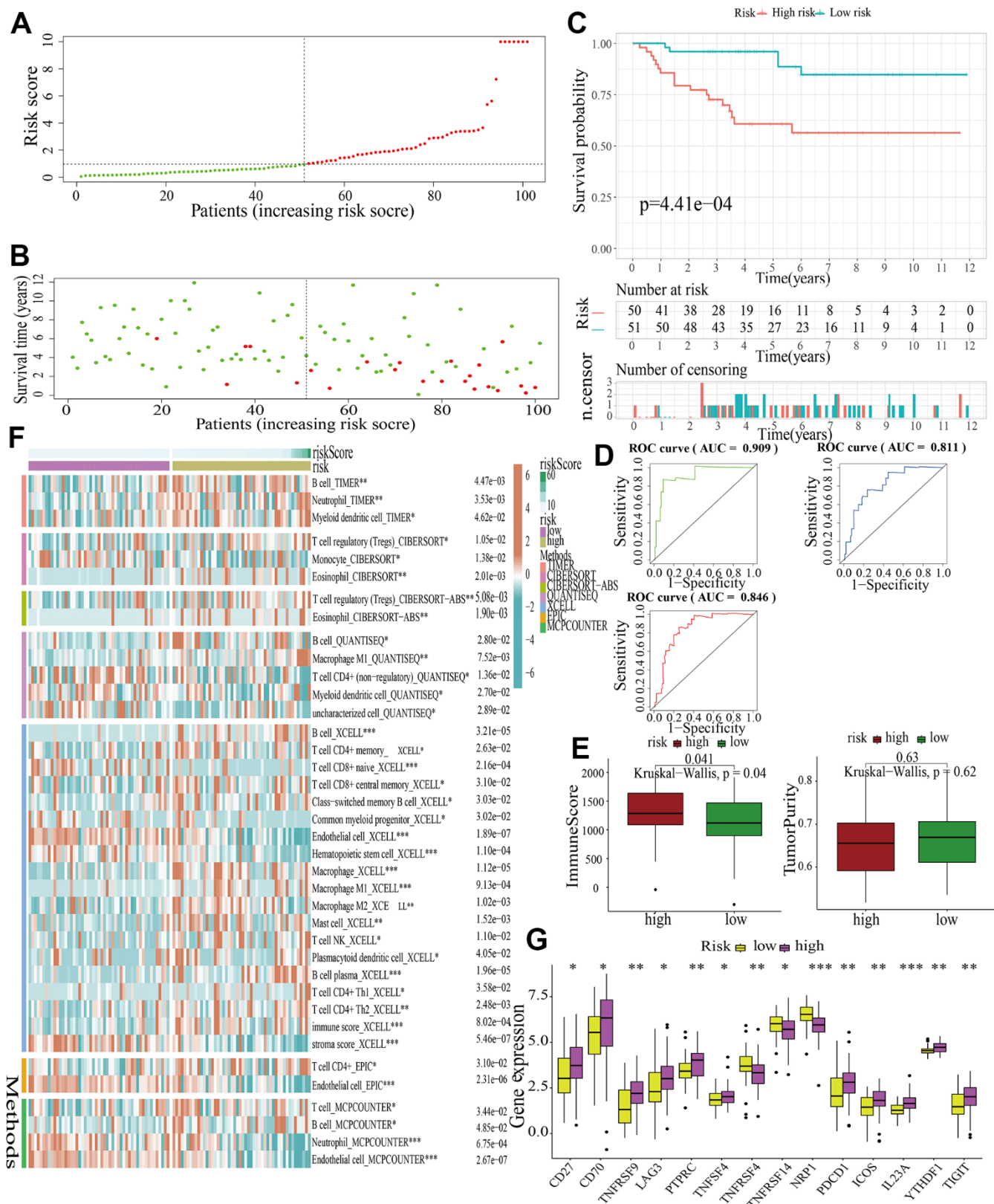
Figure 8. External validation of a MAPK-related signature in test3 cohort. (**A**) The distinguishment of high- and low-risk subgroups based on the median risk score in train cohort. (**B**) The distributions of the risk score and survival status. (**C**) Survival analysis in test3 cohort. (**D**) ROC curves of 1-, 3-, and 5-year survival. (**E**) Assessment of TME by "ESTIMATE". (**F**) The discrepancies of immune response in high- and low-risk subgroups. (**G**) The discrepancies of ICD expression in high- and low-risk subgroups.

proportion in high-risk subgroup in the three test cohorts consistently (Figures 6F, 7F, 8F). The expression levels of ICGs in high- and low-risk subgroups were also compared and it was found that CD27, CD70, TNFRSF9, LAG3, PDCD1, ICOS, IL23A, and TIGIT up-regulated while NRP1 down-regulated in the high-risk subgroup in all three test cohorts (Figures 6G, 7G, 8G).

The estimation of MAPK pathway and the expression of genes in the MAPKS in different celltypes

The scRNA-seq data of 7 KIRC samples and 5 normal samples were integrated. After the quality control (Supplementary Figure 1), 56602 cells were grouped into 43 clusters (Figure 9A and Supplementary Figure 2A, 2B). Then these clusters were defined as different cell types based on the specific markers (Figure 9B–9D and Supplementary Figure 2C). The pathway score of MAPK signaling in different cell type was estimated. It suggested that the MAPK pathway was active in each celltype. Especially, it had superior score in endothelial cells (Figure 10A). After comparing the MAPK activity of each cell type between tumor samples and normal samples, we found that the statistical discrepancies existed in myeloid, epithelial, NK, B, and endothelial cells (Figure 10B, 10C).

Identification and validation of hub genes in the occurrence of KIRC

Among all the 11 genes in the MAPKS, 3 genes showed statistically distinct mRNA expression between KIRC and normal samples. Compared with normal samples, the mRNA levels of MAP3K11 and SPRED1 increased while the mRNA level of PAPSS1 decreased in KIRC (Supplementary Figure 3A). In addition, the expression levels of the three genes were lower in advanced KIRC (Supplementary Figure 3B, 3C). Then the tissue micro-array and immunohistochemistry (IHC) was performed to demonstrate the expression level of these three genes. And the PAPSS1, MAP3K11, and SPRED1 showed lower IHC scores in KIRC compared with para-cancer samples ($p<0.05$) (Figure 11 and Supplementary Figures 4, 5).

DISCUSSION

As the major subtype of RCC, KIRC is characterized with high heterogeneity and poor prognosis [24–26]. Due to the profound influence of MAPK signaling pathway on the metabolism and progression of cancer [27–31], comprehensive alterations of MAPK-related genes in pan-cancer need to be summarized. In view of the interactions between pathways [32, 33], the

alteration of MAPK pathway activity may affect various pathways in cancer. In the study, the pan-cancer analyses about the influence of MAPK pathway revealed that the expression of many MAPK-related genes varied with the occurrence and development of cancers.

Considering the significant role of MAPK pathway in pan-cancer and the rare reports about the relationship between MAPK pathway and KIRC, we focused on the alterations of MAPK pathway and corresponding influence in KIRC. Based on the expression of the MAPK genes, KIRC samples were group into three clusters with different MAPK signaling activity. In the in-depth research, it was revealed that MAPK-active samples had higher survival rate while MAPK-inactive samples had worse survival. With different status of MAPK signaling, metabolism pathways and immune pathways showed different activities in these three clusters. MAPK signaling also showed influence on the status of various cell deaths including curroptosis, immunogenic cell death, necroptosis, apoptosis, auto-phagy, ferropotosis, phagocytosis, necrosis, pyroptosis, PANoptosis, and disulfidptosis. TME and immune response also differed in the three clusters. Most immune cells except Tfh had positive correlation with MAPK activity. Of note, the responses of mast cells, Treg, type-II-IFN, and neutrophil were positively related to the MAPK activity.

As for drug therapy, samples with different MAPK activity might have different drug sensitivity. MAPK-active samples might be sensitive to Irinotecan and Topotecan, while MAPK-inactive samples may be sensitive to Cisplatin, Cyclophosphamide, Cytarabine, Docetaxel, Gefitinib, Lapatinib, Nilotinib, Sorafenib, Temozolomide, and Vinblastine.

In view of the influence of MAPK pathway activity on KIRC in multiple respects especially survival, the following analyses aimed to identify a signature for distinguish KIRC samples with distinct prognosis and microenvironment. Among all the genes related to MAPK pathway, 11 genes (i.e., SPRED3, ACTB, ARAF, MAP3K11, PAPSS1, TLN1, CALM1, AGK, MAP2K2, MAPK1, SPRED1) were identified as hub genes and used to construct a MAPKS. Compared with normal samples, the mRNA levels of MAP3K11 and SPRED1 increased while the mRNA level of PAPSS1 decreased in KIRC. The following IHC indicated that the PAPSS1, MAP3K11, and SPRED1 showed lower IHC score in KIRC compared with para-cancer samples. The post-transcriptional modifications play an important role in the overall regulation of gene expression, which might be the reason of the inconsistent changes in protein and mRNA [34, 35].

As for all the 11 genes in MAPSK, ACTB, AGK, MAP2K2, and MAPK1 were reported to regulate RCC. A single-cell analysis reveals ACTB is involved in the regulation of RCC metastasis and progression [36]. Also, it is demonstrated as an optimal reference gene in RCC by reverse transcription PCR (RT-PCR) [37]. AGK is found to promote RCC progression via activating the PI3K/AKT/GSK3β signalling pathway [38]. MAP2K2, another regulator of RCC, can promote its progression by affecting transcriptional activation of
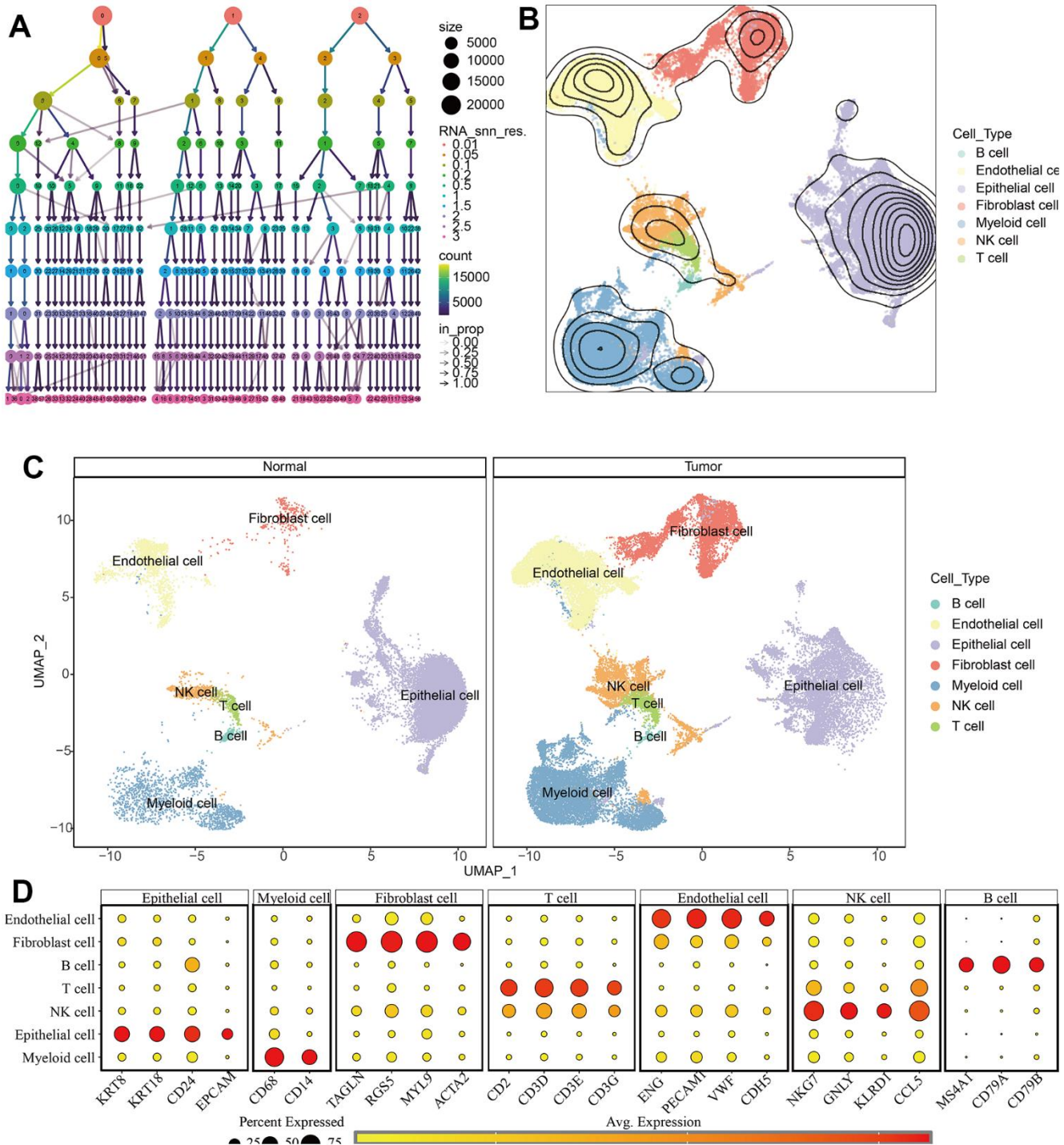
Figure 9. Identification of different cell types in KIRC and normal samples. (**A**) The clustree for identifying suitable cell clusters. (**B**) Different types of cells in all samples. (**C**) Different types of cells in KIRC and normal samples. (**D**) The expression of marker genes in each cell type.

the MAP2K2-dependent ERK pathway [39]. MAPK1, one of the members of MAPK family, promotes RCC metastasis through HCP5/miR-214-3p/MAPK1 axis [40]. SPRED1, as a negative regulator of the MAPK pathway [41], influences tumor growth and metastasis in breast cancer. Also, the overexpression of SPRED1 can inhibit the proliferation, migration and invasion of HCC [42]. SPRED3, is reported to have an

influence on EGFR mutated NSCLC [43], glioblastoma [44], and cervical carcinoma [45]. ARAF, is reported to be an oncogene in gallbladder cancer [46]. Its mutations imply resistance to the RAF inhibitor belvarafenib in melanoma [47]. In addition, mutant ARAF is found to be an oncogenic driver in lung adenocarcinoma and can be used as an indicator of sorafenib response [48]. MAP3K11 acts as a tumor suppressor [49] and a driver
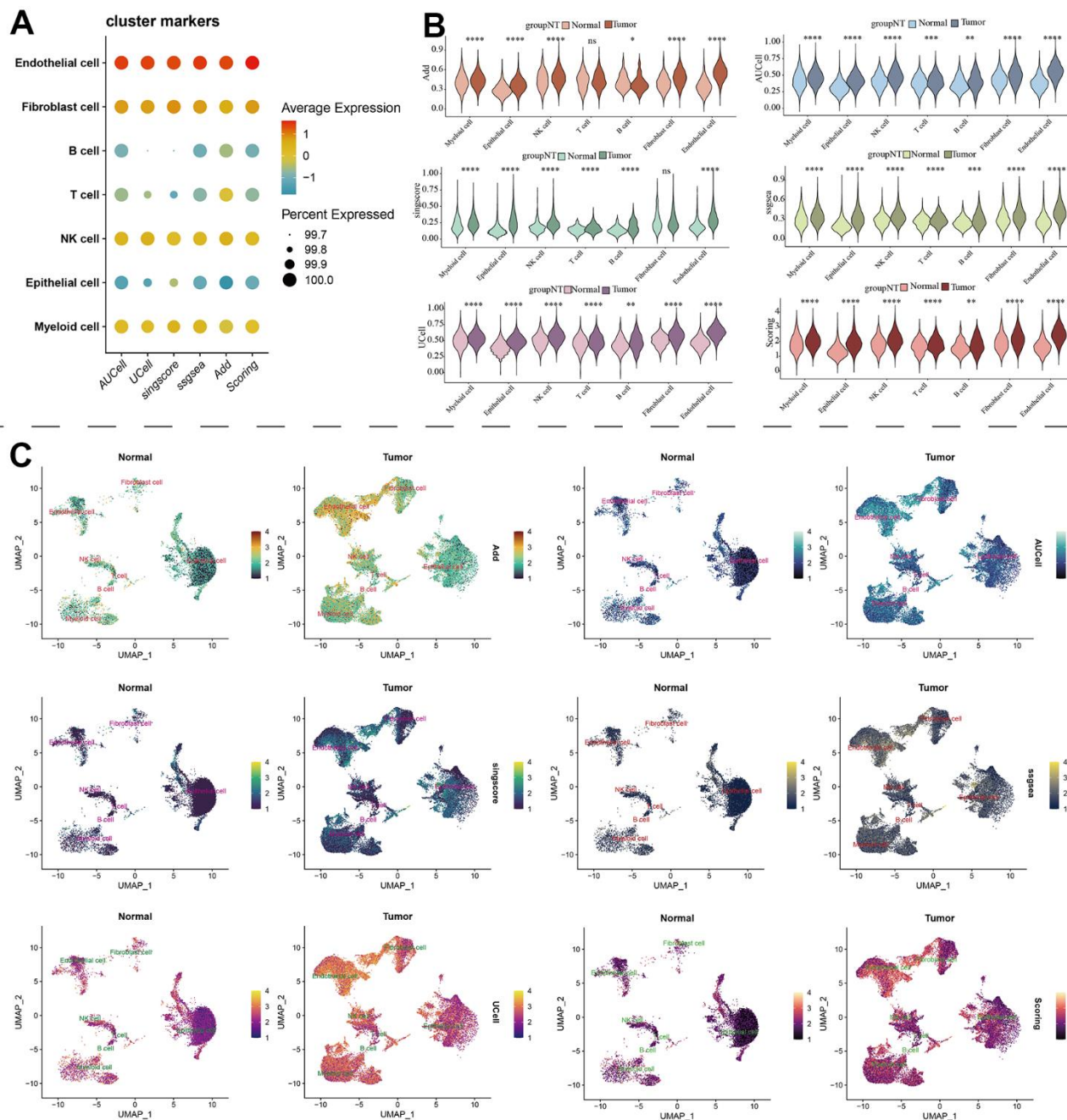

Figure 10. The estimation of MAPK pathway based on scRNA-Seq data. (**A**) The pathway score of MAPK signaling in each cell type; (**B**) The discrepancies of MAPK score in each cell type between KIRC and normal samples; (**C**) The detailed MAPK pathway activity shown in a UMAP plot.

of cancer cachexia [50]. Also, it can regulate the malignancy of oral squamous cell carcinoma through facilitating autophagy [51]. Through regulating MAP3K11, NSCLC can be suppressed [52]. PAPSS1 is demonstrated as a suppressor gene in esophageal squamous cancer [53]. Out of this, it is reported to be associated with breast tumors previously [54]. TLN1, locating in focal adhesion, can regulate integrin signaling and promote cancer metastasis [55–58]. It can affect cell proliferation and differentiation in acute myeloid leukemia [59], define the risk of aggressive oral squamous cell carcinoma [60], and act as a regulator to suppress ovarian serous carcinoma [61]. CALM1 can engage in the formation of calmodulin and regulate proliferation, motility and differentiation through participating in signaling pathways [62]. Studies revealed that the expression of CALM1 was significantly linked to many types of cancer, such as prostate cancer [63], bladder cancer [64], and nasopharyngeal carcinoma [65].
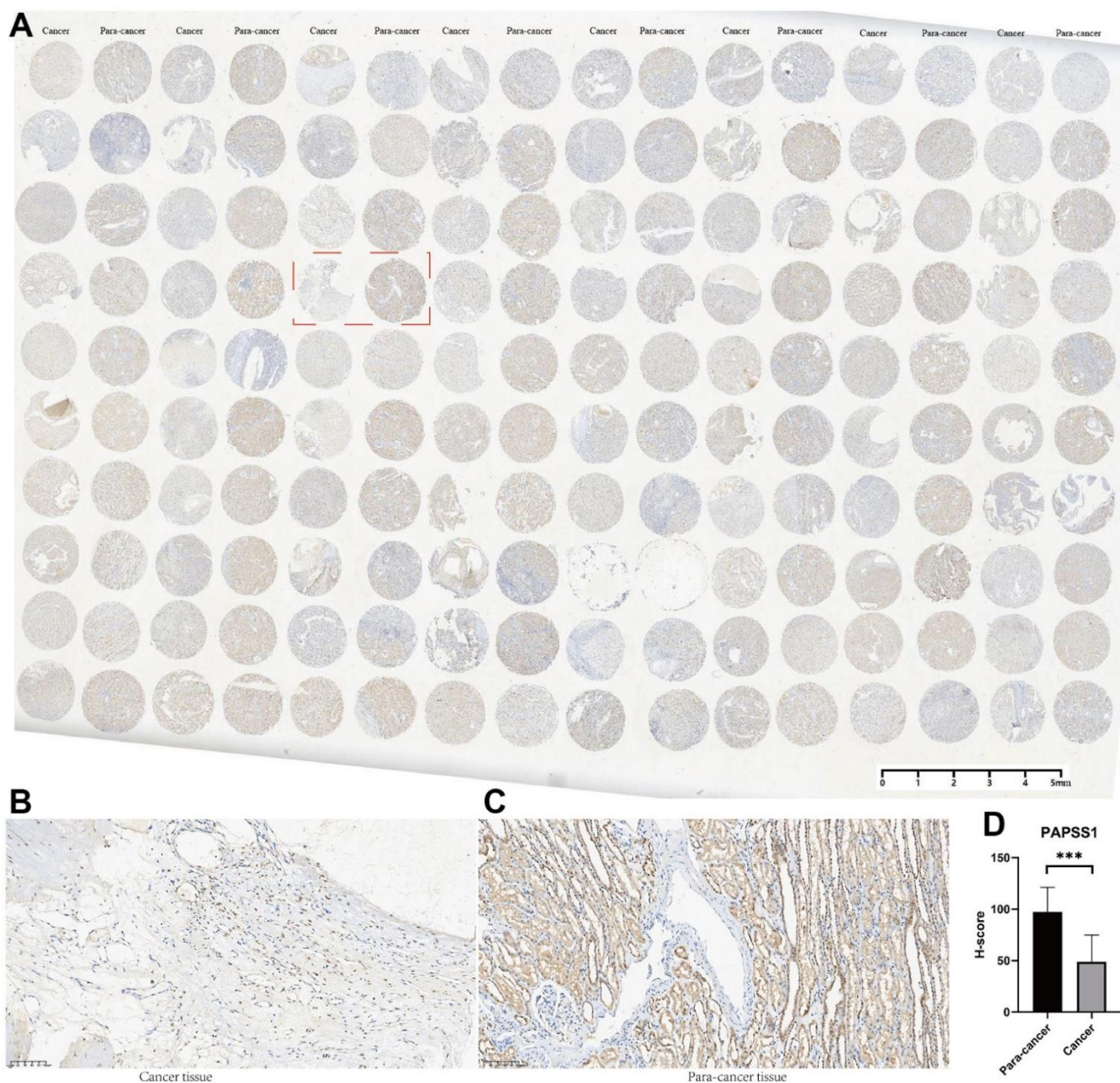

Figure 11. The tissue microarray and immunohistochemistry (IHC) of PAPSS1. (A) Immunohistochemical maps for all samples. (B) Immunohistochemical maps of typical cancer samples. (C) Immunohistochemical maps of typical para-cancer samples. (D) Immunohistochemical statistical analysis results.

Based on the MAPKS, the risk scores of all KIRC samples were calculated and two subgroups (i.e., high-risk subgroup and low-risk subgroup) were obtained in accordance with the risk score of the train cohort. The MAPKS helped to differentiate high-risk samples characterized by lower survival rates, higher immune scores, and reduced tumor purities. Of note, the elevated presence of Treg cells and the atypical expression of immune checkpoint molecules could potentially contribute to its adverse prognosis. As is reported, Treg cells can suppress effective tumor immunity. It was found that increasing infiltration of Treg cells was linked to poor prognosis of patients with tumors [66, 67]. In addition, tumor cells could disguise themselves as common components of the human body through immune checkpoint pathways [68]. As a consequence, the up-regulation of most ICGs in high-risk sub-group might account for the poor prognosis. All the discrepancies might be the potential therapy targets in KIRC and all the results above were demonstrated in the three test cohorts. In addition, the single-cell RNA sequencing (scRNA-seq) analysis of KIRC samples identified seven distinct cell types, which include B cells, myeloid cells, endothelial cells, NK cells, epithelial cells, T cells, and fibroblast cells. Endothelial cells in tumor tissues had obviously higher MAPK scores than normal tissues.

It is no doubt that a great signature MAPKS was constructed successfully. But there are still some limitations that need to be considered. First, the MAPKS was constructed utilizing a small number of KIRC samples from the TCGA and ArrayExpress databases. Then the results were obtained by utilizing bioinformatics researches. In the future, a large number of clinical samples need to be involved and fundamental experiments are necessary to utilize for further demonstration.

CONCLUSIONS

With the development of tumors, MAPK pathway altered significantly in pan-cancer. Especially in KIRC, the status of MAPK pathway linked to the survival rate and drug sensitivity. The MAPKS was successfully constructed and demonstrated to help distinguish KIRC samples into different subgroups with distinct prognosis and tumor microenvironment. All the findings will contribute to the individualized treatment in KIRC.

AUTHOR CONTRIBUTIONS

All the authors took part in the study design, data collection, data analysis, manuscript writing and revising. Dr. Xiunan Li performed IHC experiments.

CONFLICTS OF INTEREST

None of the authors have any financial or other competing interests that need to be disclosed.

FUNDING

REFERENCES

1. Hsieh JJ, Purdue MP, Signoretti S, Swanton C, Albiges L, Schmidinger M, Heng DY, Larkin J, Ficarra V. Renal cell carcinoma. Nat Rev Dis Primers. 2017; 3:17009.
https://doi.org/10.1038/nrdp.2017.9 PMID:28276433

2. Zhang D, Zeng S, Hu X. Identification of a three-long noncoding RNA prognostic model involved competitive endogenous RNA in kidney renal clear cell carcinoma. Cancer Cell Int. 2020; 20:319.
https://doi.org/10.1186/s12935-020-01423-4
PMID:32694941

3. Makhov P, Joshi S, Ghatalia P, Kutikov A, Uzzo RG, Kolenko VM. Resistance to Systemic Therapies in Clear Cell Renal Cell Carcinoma: Mechanisms and Management Strategies. Mol Cancer Ther. 2018; 17:1355–64.
https://doi.org/10.1158/1535-7163.MCT-17-1299
PMID:29967214

4. Degirmenci U, Wang M, Hu J. Targeting Aberrant RAS/RAF/MEK/ERK Signaling for Cancer Therapy. Cells. 2020; 9:198.
https://doi.org/10.3390/cells9010198 PMID:31941155

5. Park HB, Baek KH. E3 ligases and deubiquitinating enzymes regulating the MAPK signaling pathway in cancers. Biochim Biophys Acta Rev Cancer. 2022; 1877:188736.
https://doi.org/10.1016/j.bbcan.2022.188736
PMID:35589008

6. Fang JY, Richardson BC. The MAPK signalling pathways and colorectal cancer. Lancet Oncol. 2005; 6:322–7.
https://doi.org/10.1016/S1470-2045(05)70168-6
PMID:15863380

7. Anjum J, Mitra S, Das R, Alam R, Mojumder A, Emran TB, Islam F, Rauf A, Hossain MJ, Aljohani AS, Abdulmonem WA, Alsharif KF, Alzahrani KJ, Khan H. A renewed concept on the MAPK signaling pathway in cancers: Polyphenols as a choice of therapeutics. Pharmacol Res. 2022; 184:106398.
https://doi.org/10.1016/j.phrs.2022.106398
PMID:35988867

8. Zhang MH, Wong JH, Liu F, Ng TB, Liu ZK. Fungal antitumor protein D1 is internalized via endocytosis

and inhibits non-small cell lung cancer proliferation through MAPK signaling pathway. Int J Biol Macromol. 2023; 227:45–57.
https://doi.org/10.1016/j.ijbiomac.2022.12.061
PMID:36521713

9. Lee S, Rauch J, Kolch W. Targeting MAPK Signaling in Cancer: Mechanisms of Drug Resistance and Sensitivity. Int J Mol Sci. 2020; 21:1102.
https://doi.org/10.3390/ijms21031102
PMID:32046099

10. Hu FF, Liu CJ, Liu LL, Zhang Q, Guo AY. Expression profile of immune checkpoint genes and their roles in predicting immunotherapy response. Brief Bioinform. 2021; 22:bbaa176.
https://doi.org/10.1093/bib/bbaa176
PMID:32814346

11. Drosten M, Barbacid M. Targeting the MAPK Pathway in KRAS-Driven Tumors. Cancer Cell. 2020; 37:543–50.
https://doi.org/10.1016/j.ccell.2020.03.013
PMID:32289276

12. Burotto M, Chiou VL, Lee JM, Kohn EC. The MAPK pathway across different malignancies: a new perspective. Cancer. 2014; 120:3446–56.
https://doi.org/10.1002/cncr.28864
PMID:24948110

13. Santarpia L, Lippman SM, El-Naggar AK. Targeting the MAPK-RAS-RAF signaling pathway in cancer therapy. Expert Opin Ther Targets. 2012; 16:103–19.
https://doi.org/10.1517/14728222.2011.645805
PMID:22239440

14. Wei J, Liu R, Hu X, Liang T, Zhou Z, Huang Z. MAPK signaling pathway-targeted marine compounds in cancer therapy. J Cancer Res Clin Oncol. 2021; 147:3–22.
https://doi.org/10.1007/s00432-020-03460-y
PMID:33389079

15. Dong Y, Yuan Q, Ren J, Li H, Guo H, Guan H, Jiang X, Qi B, Li R. Identification and characterization of a novel molecular classification incorporating oxidative stress and metabolism-related genes for stomach adenocarcinoma in the framework of predictive, preventive, and personalized medicine. Front Endocrinol (Lausanne). 2023; 14:1090906.
https://doi.org/10.3389/fendo.2023.1090906
PMID:36860371

16. Cui Y, Yuan Q, Chen J, Jiang J, Guan H, Zhu R, Li N, Liu W, Wang C. Determination and characterization of molecular heterogeneity and precision medicine strategies of patients with pancreatic cancer and pancreatic neuroendocrine tumor based on oxidative stress and mitochondrial dysfunction-related genes. Front Endocrinol (Lausanne). 2023; 14:1127441.

https://doi.org/10.3389/fendo.2023.1127441
PMID:37223030

17. Li N, Jia X, Wang Z, Wang K, Qu Z, Chi D, Sun Z, Jiang J, Cui Y, Wang C. Characterization of anoikis-based molecular heterogeneity in pancreatic cancer and pancreatic neuroendocrine tumor and its association with tumor immune microenvironment and metabolic remodeling. Front Endocrinol (Lausanne). 2023; 14:1153909.
https://doi.org/10.3389/fendo.2023.1153909
PMID:37234801

18. Ma Y, Yuan Q, He S, Mao X, Zheng S, Chen C. Characterizing the prognostic and therapeutic value of necroptosis in sarcoma based on necroptosis subtypes. Front Genet. 2022; 13:980209.
https://doi.org/10.3389/fgene.2022.980209
PMID:36238158

19. Zhang B, Yuan Q, Zhang B, Li S, Wang Z, Liu H, Meng F, Chen X, Shang D. Characterization of neuroendocrine regulation- and metabolism-associated molecular features and prognostic indicators with aid to clinical chemotherapy and immunotherapy of patients with pancreatic cancer. Front Endocrinol (Lausanne). 2023; 13:1078424.
https://doi.org/10.3389/fendo.2022.1078424
PMID:36743929

20. Zhang P, Pei S, Gong Z, Feng Y, Zhang X, Yang F, Wang W. By integrating single-cell RNA-seq and bulk RNA-seq in sphingolipid metabolism, CACYBP was identified as a potential therapeutic target in lung adenocarcinoma. Front Immunol. 2023; 14:1115272.
https://doi.org/10.3389/fimmu.2023.1115272
PMID:36776843

21. Zhang P, Pei S, Wu L, Xia Z, Wang Q, Huang X, Li Z, Xie J, Du M, Lin H. Integrating multiple machine learning methods to construct glutamine metabolism-related signatures in lung adenocarcinoma. Front Endocrinol (Lausanne). 2023; 14:1196372.
https://doi.org/10.3389/fendo.2023.1196372
PMID:37265698

22. Stuart T, Butler A, Hoffman P, Hafemeister C, Papalexi E, Mauck WM 3rd, Hao Y, Stoeckius M, Smibert P, Satija R. Comprehensive Integration of Single-Cell Data. Cell. 2019; 177:1888–902.e21.
https://doi.org/10.1016/j.cell.2019.05.031
PMID:31178118

23. Motzer RJ, Jonasch E, Agarwal N, Alva A, Baine M, Beckermann K, Carlo MI, Choueiri TK, Costello BA, Derweesh IH, Desai A, Ged Y, George S, et al. Kidney Cancer, Version 3.2022, NCCN Clinical Practice Guidelines in Oncology. J Natl Compr Canc Netw. 2022; 20:71–90.

https://doi.org/10.6004/jnccn.2022.0001
PMID:34991070

24. Motzer RJ, Jonasch E, Agarwal N, Beard C, Bhayani S, Bolger GB, Chang SS, Choueiri TK, Costello BA, Derweesh IH, Gupta S, Hancock SL, Kim JJ, et al, and National comprehensive cancer network. Kidney cancer, version 3.2015. J Natl Compr Canc Netw. 2015; 13:151–9.
https://doi.org/10.6004/jnccn.2015.0022
PMID:25691606

25. Miller KD, Nogueira L, Mariotto AB, Rowland JH, Yabroff KR, Alfano CM, Jemal A, Kramer JL, Siegel RL. Cancer treatment and survivorship statistics, 2019. CA Cancer J Clin. 2019; 69:363–85.
https://doi.org/10.3322/caac.21565 PMID:31184787

26. Majer W, Kluzek K, Bluyssen H, Wesoły J. Potential Approaches and Recent Advances in Biomarker Discovery in Clear-Cell Renal Cell Carcinoma. J Cancer. 2015; 6:1105–13.
https://doi.org/10.7150/jca.12145
PMID:26516358

27. Asl ER, Amini M, Najafi S, Mansoori B, Mokhtarzadeh A, Mohammadi A, Lotfinejad P, Bagheri M, Shirjang S, Lotfi Z, Rasmi Y, Baradaran B. Interplay between MAPK/ERK signaling pathway and MicroRNAs: A crucial mechanism regulating cancer cell metabolism and tumor progression. Life Sci. 2021; 278:119499.
https://doi.org/10.1016/j.lfs.2021.119499
PMID:33865878

28. Han Z, Liu D, Chen L, He Y, Tian X, Qi L, Chen L, Luo Y, Chen Z, Hu X, Li G, Zhan L, Wang Y, et al. PNO1 regulates autophagy and apoptosis of hepatocellular carcinoma via the MAPK signaling pathway. Cell Death Dis. 2021; 12:552.
https://doi.org/10.1038/s41419-021-03837-y
PMID:34050137

29. Mu W, Jia Y, Chen X, Li H, Wang Z, Cheng B. Intracellular Porphyromonas gingivalis Promotes the Proliferation of Colorectal Cancer Cells via the MAPK/ERK Signaling Pathway. Front Cell Infect Microbiol. 2020; 10:584798.
https://doi.org/10.3389/fcimb.2020.584798
PMID:33425779

30. Chen Z, Jiang Z, Meng L, Wang Y, Lin M, Wei Z, Han W, Ying S, Xu A. SAMHD1, positively regulated by KLF4, suppresses the proliferation of gastric cancer cells through MAPK p38 signaling pathway. Cell Cycle. 2022; 21:2065–78.
https://doi.org/10.1080/15384101.2022.2085356
PMID:35670736

31. Wang M, Tian B, Shen J, Xu S, Liu C, Guan L, Guo M, Dou J. Bavachin induces apoptosis in colorectal cancer cells through Gadd45a via the MAPK signaling pathway. Chin J Nat Med. 2023; 21:36–46.
https://doi.org/10.1016/S1875-5364(23)60383-8
PMID:36641231

32. Visakh R, Abdul Nazeer KA. Identifying epigenetically dysregulated pathways from pathway-pathway interaction networks. Comput Biol Med. 2016; 76:160–7.
https://doi.org/10.1016/j.compbiomed.2016.06.030
PMID:27454244

33. Hsu CL, Yang UC. Discovering pathway cross-talks based on functional relations between pathways. BMC Genomics. 2012 (Suppl 7); 13:S25.
https://doi.org/10.1186/1471-2164-13-S7-S25
PMID:23282018

34. Nachtergaele S, He C. The emerging biology of RNA post-transcriptional modifications. RNA Biol. 2017; 14:156–63.
https://doi.org/10.1080/15476286.2016.1267096
PMID:27937535

35. Zhao BS, Roundtree IA, He C. Post-transcriptional gene regulation by mRNA modifications. Nat Rev Mol Cell Biol. 2017; 18:31–42.
https://doi.org/10.1038/nrm.2016.132
PMID:27808276

36. Liu K, Gao R, Wu H, Wang Z, Han G. Single-cell analysis reveals metastatic cell heterogeneity in clear cell renal cell carcinoma. J Cell Mol Med. 2021; 25:4260–74.
https://doi.org/10.1111/jcmm.16479 PMID:33759378

37. Glenn ST, Jones CA, Liang P, Kaushik D, Gross KW, Kim HL. Expression profiling of archival renal tumors by quantitative PCR to validate prognostic markers. Biotechniques. 2007; 43:639–40.
https://doi.org/10.2144/000112562
PMID:18072593

38. Zhu Q, Zhong AL, Hu H, Zhao JJ, Weng DS, Tang Y, Pan QZ, Zhou ZQ, Song MJ, Yang JY, He JY, Liu Y, Li M, et al. Acylglycerol kinase promotes tumour growth and metastasis via activating the PI3K/AKT/GSK3β signalling pathway in renal cell carcinoma. J Hematol Oncol. 2020; 13:2.
https://doi.org/10.1186/s13045-019-0840-4
PMID:31900208

39. Ren LX, Qi JC, Zhao AN, Shi B, Zhang H, Wang DD, Yang Z. Myc-associated zinc-finger protein promotes clear cell renal cell carcinoma progression through transcriptional activation of the MAP2K2-dependent ERK pathway. Cancer Cell Int. 2021; 21:323.
https://doi.org/10.1186/s12935-021-02020-9
PMID:34183010

40. Hao JF, Chen P, Li HY, Li YJ, Zhang YL. Effects of LncRNA HCP5/miR-214-3p/MAPK1 Molecular Network on

Renal Cell Carcinoma Cells. Cancer Manag Res. 2020; 12:13347–56.
https://doi.org/10.2147/CMAR.S274426
PMID:33380840

41. Nonami A, Kato R, Taniguchi K, Yoshiga D, Taketomi T, Fukuyama S, Harada M, Sasaki A, Yoshimura A. Spred-1 negatively regulates interleukin-3-mediated ERK/mitogen-activated protein (MAP) kinase activation in hematopoietic cells. J Biol Chem. 2004; 279:52543–51.
https://doi.org/10.1074/jbc.M405189200
PMID:15465815

42. Yoshida T, Hisamoto T, Akiba J, Koga H, Nakamura K, Tokunaga Y, Hanada S, Kumemura H, Maeyama M, Harada M, Ogata H, Yano H, Kojiro M, et al. Spreds, inhibitors of the Ras/ERK signal transduction, are dysregulated in human hepatocellular carcinoma and linked to the malignant phenotype of tumors. Oncogene. 2006; 25:6056–66.
https://doi.org/10.1038/sj.onc.1209635
PMID:16652141

43. He Z, Gong F, Liao J, Wang Q, Su Y, Chen C, Lin J, Lin RJ. Spred-3 mutation and Ras/Raf/MAPK activation confer acquired resistance to EGFR tyrosine kinase inhibitor in an EGFR mutated NSCLC cell line. Transl Cancer Res. 2020; 9:2542–55.
https://doi.org/10.21037/tcr.2020.03.05
PMID:35117614

44. Mizoguchi M, Nutt CL, Louis DN. Mutation analysis of CBL-C and SPRED3 on 19q in human glioblastoma. Neurogenetics. 2004; 5:81–2.
https://doi.org/10.1007/s10048-003-0164-x
PMID:14618415

45. Halle MK, Sundaresan A, Zhang J, Pedamallu CS, Srinivasasainagendra V, Blair J, Brooke D, Bertelsen BI, Woie K, Shrestha S, Tiwari H, Wong YF, Krakstad C, Ojesina AI. Genomic alterations associated with mutational signatures, DNA damage repair and chromatin remodeling pathways in cervical carcinoma. NPJ Genom Med. 2021; 6:82.
https://doi.org/10.1038/s41525-021-00244-2
PMID:34620846

46. Lin W, Tong C, Zhang W, Cen W, Wang Y, Li J, Zhu Z, Yu J, Lu B. Silencing ARAF Suppresses the Malignant Phenotypes of Gallbladder Cancer Cells. Biomed Res Int. 2020; 2020:3235786.
https://doi.org/10.1155/2020/3235786
PMID:32923479

47. Yen I, Shanahan F, Lee J, Hong YS, Shin SJ, Moore AR, Sudhamsu J, Chang MT, Bae I, Dela Cruz D, Hunsaker T, Klijn C, Liau NP, et al. ARAF mutations confer resistance to the RAF inhibitor belvarafenib in melanoma. Nature. 2021; 594:418–23.

https://doi.org/10.1038/s41586-021-03515-1
PMID:33953400

48. Imielinski M, Greulich H, Kaplan B, Araujo L, Amann J, Horn L, Schiller J, Villalona-Calero MA, Meyerson M, Carbone DP. Oncogenic and sorafenib-sensitive ARAF mutations in lung adenocarcinoma. J Clin Invest. 2014; 124:1582–6.
https://doi.org/10.1172/JCI72763 PMID:24569458

49. Knackmuss U, Lindner SE, Aneichyk T, Kotkamp B, Knust Z, Villunger A, Herzog S. MAP3K11 is a tumor suppressor targeted by the oncomiR miR-125b in early B cells. Cell Death Differ. 2016; 23:242–52.
https://doi.org/10.1038/cdd.2015.87 PMID:26138442

50. Lerner L, Tao J, Liu Q, Nicoletti R, Feng B, Krieger B, Mazsa E, Siddiquee Z, Wang R, Huang L, Shen L, Lin J, Vigano A, et al. MAP3K11/GDF15 axis is a critical driver of cancer cachexia. J Cachexia Sarcopenia Muscle. 2016; 7:467–82.
https://doi.org/10.1002/jcsm.12077 PMID:27239403

51. Liu PF, Chen CF, Ger LP, Tsai WL, Tseng HH, Lee CH, Yang WH, Shu CW. MAP3K11 facilitates autophagy activity and is correlated with malignancy of oral squamous cell carcinoma. J Cell Physiol. 2022; 237:4275–91.
https://doi.org/10.1002/jcp.30881 PMID:36103355

52. Li Y, Wang D, Li X, Shao Y, He Y, Yu H, Ma Z. MiR-199a-5p suppresses non-small cell lung cancer via targeting MAP3K11. J Cancer. 2019; 10:2472–9.
https://doi.org/10.7150/jca.29426 PMID:31258753

53. Zhu X, Zhu P, Chen X, Zhang L, Wu C, Zhang H, Shen X, Qi Y, Chen M, Wang S, Yi X. Correlation of 3'-phosphoadenosine-5'-phosphosulfate synthase 1 (PAPSS1) expression with clinical parameters and prognosis in esophageal squamous cell carcinoma. Histol Histopathol. 2023; 38:1327–35.
https://doi.org/10.14670/HH-18-590 PMID:36734141

54. Segaert P, Lopes MB, Casimiro S, Vinga S, Rousseeuw PJ. Robust identification of target genes and outliers in triple-negative breast cancer data. Stat Methods Med Res. 2019; 28:3042–56.
https://doi.org/10.1177/0962280218794722
PMID:30146936

55. Desiniotis A, Kyprianou N. Significance of talin in cancer progression and metastasis. Int Rev Cell Mol Biol. 2011; 289:117–47.
https://doi.org/10.1016/B978-0-12-386039-2.00004-3
PMID:21749900

56. Hoshino A, Costa-Silva B, Shen TL, Rodrigues G, Hashimoto A, Tesic Mark M, Molina H, Kohsaka S, Di Giannatale A, Ceder S, Singh S, Williams C, Soplop N, et al. Tumour exosome integrins determine organotropic metastasis. Nature. 2015; 527:329–35.
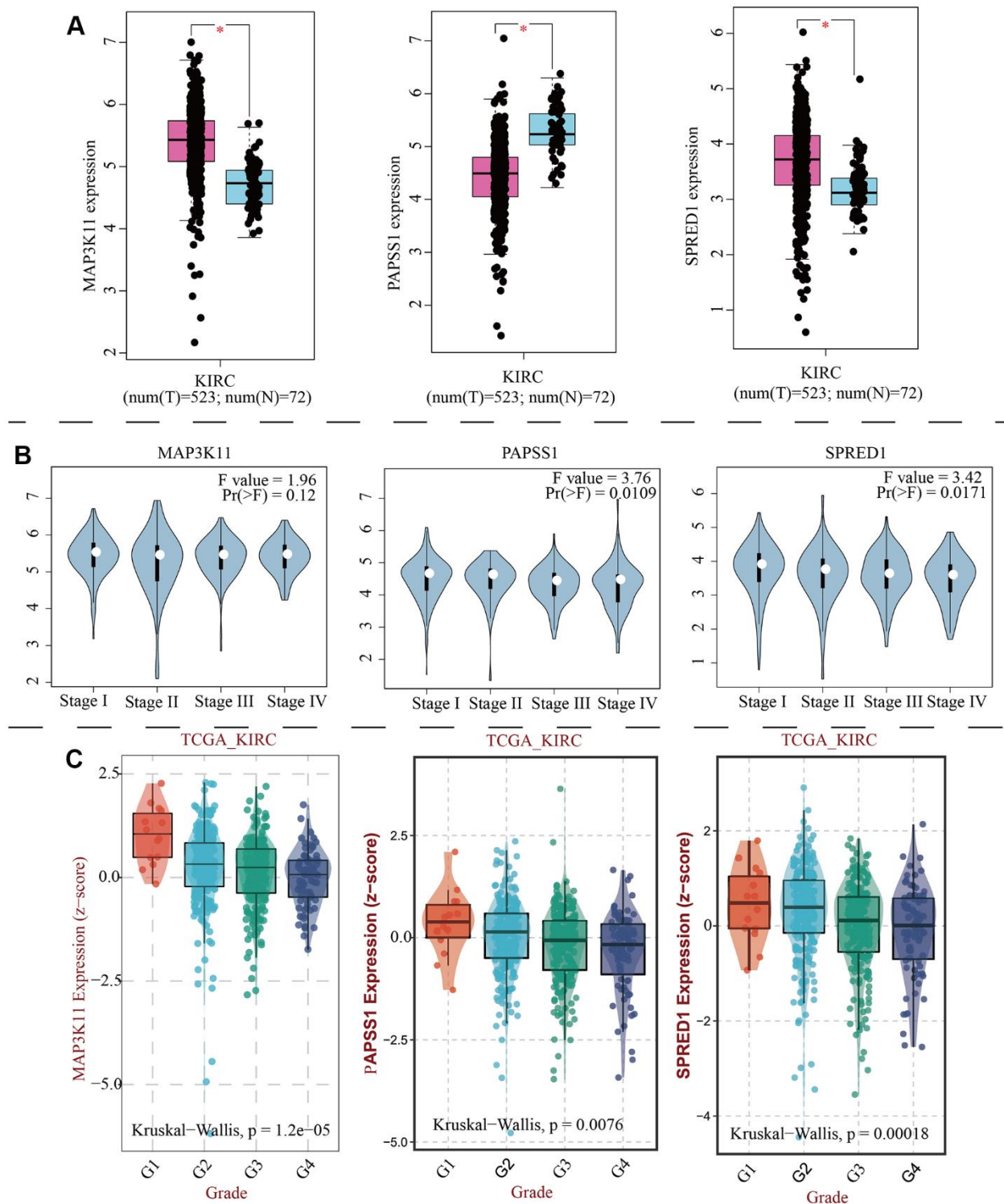
https://doi.org/10.1038/nature15756
PMID:26524530

57. Klapholz B, Brown NH. Talin - the master of integrin adhesions. J Cell Sci. 2017; 130:2435–46.
https://doi.org/10.1242/jcs.190991 PMID:28701514

58. Seguin L, Desgrosellier JS, Weis SM, Cheresh DA. Integrins and cancer: regulators of cancer stemness, metastasis, and drug resistance. Trends Cell Biol. 2015; 25:234–40.
https://doi.org/10.1016/j.tcb.2014.12.006
PMID:25572304

59. Cui D, Cui X, Xu X, Zhang W, Yu Y, Gao Y, Mei C, Zheng W. Identification of TLN1 as a prognostic biomarker to effect cell proliferation and differentiation in acute myeloid leukemia. BMC Cancer. 2022; 22:1027.
https://doi.org/10.1186/s12885-022-10099-0
PMID:36175877

60. Lai MT, Hua CH, Tsai MH, Wan L, Lin YJ, Chen CM, Chiu IW, Chan C, Tsai FJ, Jinn-Chyuan Sheu J. Talin-1 overexpression defines high risk for aggressive oral squamous cell carcinoma and promotes cancer metastasis. J Pathol. 2011; 224:367–76.
https://doi.org/10.1002/path.2867 PMID:21547905

61. Tang H, Yao L, Tao X, Yu Y, Chen M, Zhang R, Xu C. miR-9 functions as a tumor suppressor in ovarian serous carcinoma by targeting TLN1. Int J Mol Med. 2013; 32:381–8.
https://doi.org/10.3892/ijmm.2013.1400
PMID:23722670

62. Chin D, Means AR. Calmodulin: a prototypical calcium sensor. Trends Cell Biol. 2000; 10:322–8.
https://doi.org/10.1016/s0962-8924(00)01800-6
PMID:10884684

63. Adeola HA, Smith M, Kaestner L, Blackburn JM, Zerbini LF. Novel potential serological prostate cancer biomarkers using CT100+ cancer antigen microarray platform in a multi-cultural South African cohort. Oncotarget. 2016; 7:13945–64.
https://doi.org/10.18632/oncotarget.7359
PMID:26885621

64. Zhang L, Feng C, Zhou Y, Zhou Q. Dysregulated genes targeted by microRNAs and metabolic pathways in bladder cancer revealed by bioinformatics methods. Oncol Lett. 2018; 15:9617–24.
https://doi.org/10.3892/ol.2018.8602
PMID:29928337

65. Zamanian Azodi M, Rezaei Tavirani M, Rezaei Tavirani M, Vafaee R, Rostami-Nejad M. Nasopharyngeal Carcinoma Protein Interaction Mapping Analysis via Proteomic Approaches. Asian Pac J Cancer Prev. 2018; 19:845–51.
https://doi.org/10.22034/APJCP.2018.19.3.845
PMID:29582644

66. Tanaka A, Sakaguchi S. Targeting Treg cells in cancer immunotherapy. Eur J Immunol. 2019; 49:1140–6.
https://doi.org/10.1002/eji.201847659
PMID:31257581

67. Tanaka A, Sakaguchi S. Regulatory T cells in cancer immunotherapy. Cell Res. 2017; 27:109–18.
https://doi.org/10.1038/cr.2016.151
PMID:27995907

68. Li B, Chan HL, Chen P. Immune Checkpoint Inhibitors: Basics and Challenges. Curr Med Chem. 2019; 26:3009–25.
https://doi.org/10.2174/0929867324666170804143706
PMID:28782469

Supplementary Figures
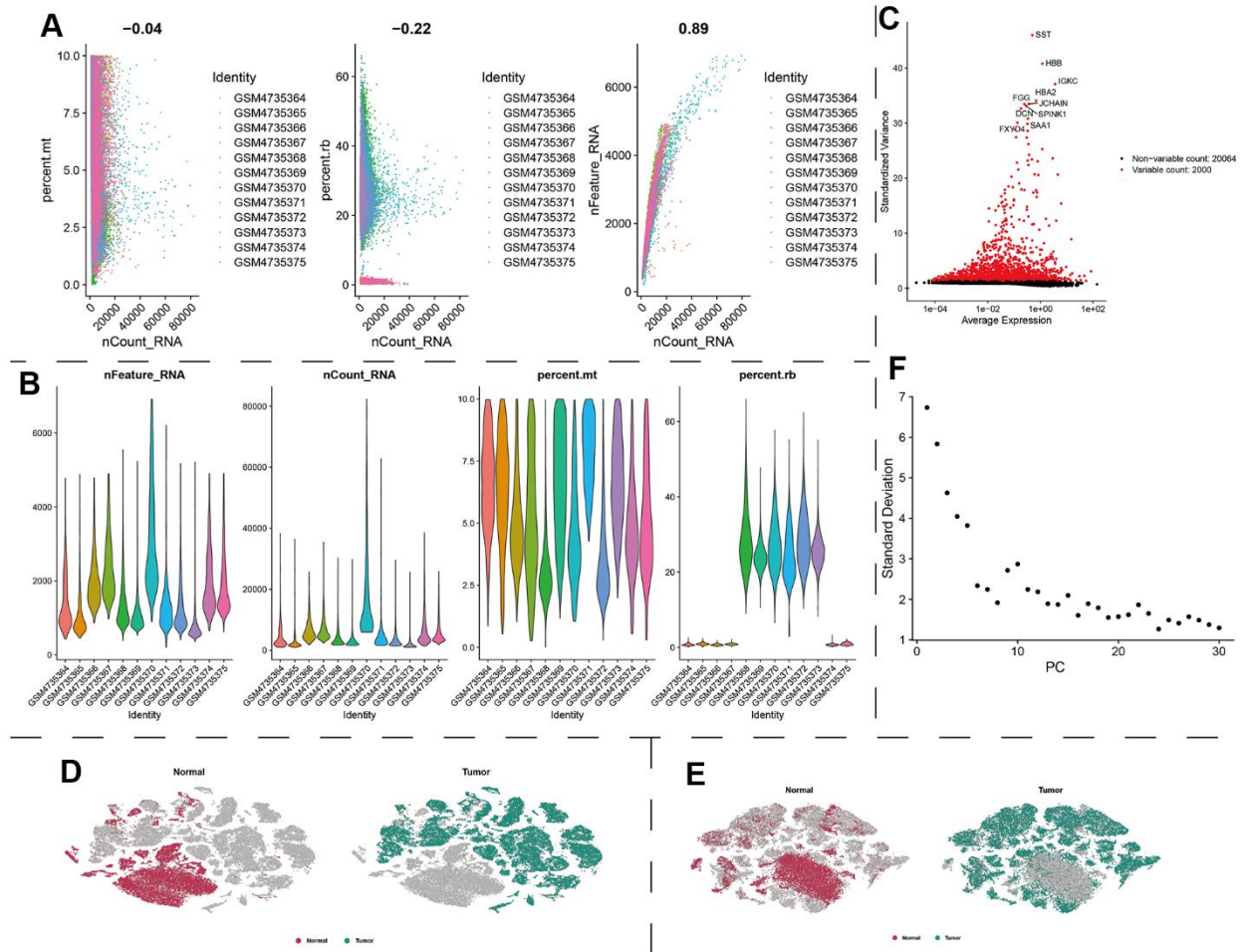
Supplementary Figure 1. Single-cell data processing. (**A**, **B**) Data quality control of sc-RNA data. (**C**) Highly variable genes of the data. (**D**, **E**) Cell distribution before and after removing the batch effect by Harmony. (**F**) ElbowPlot for identifying suitable PC number.

Supplementary Figure 2. Single-cell dimension reduction and annotation process. (**A**) UMAP dimension reduction plots for all samples. (**B**) UMAP dimension reduction plots for normal and tumor groups. (**C**) Single-cell annotation process.

Supplementary Figure 3. Identification of hub genes in the occurrence of KIRC. (**A**) The mRNA expression of hub genes. (**B**) The relationship between the expression of each hub gene and tumor stage in KIRC. (**C**) The relationship between the expression of each hub gene and tumor grade in KIRC.
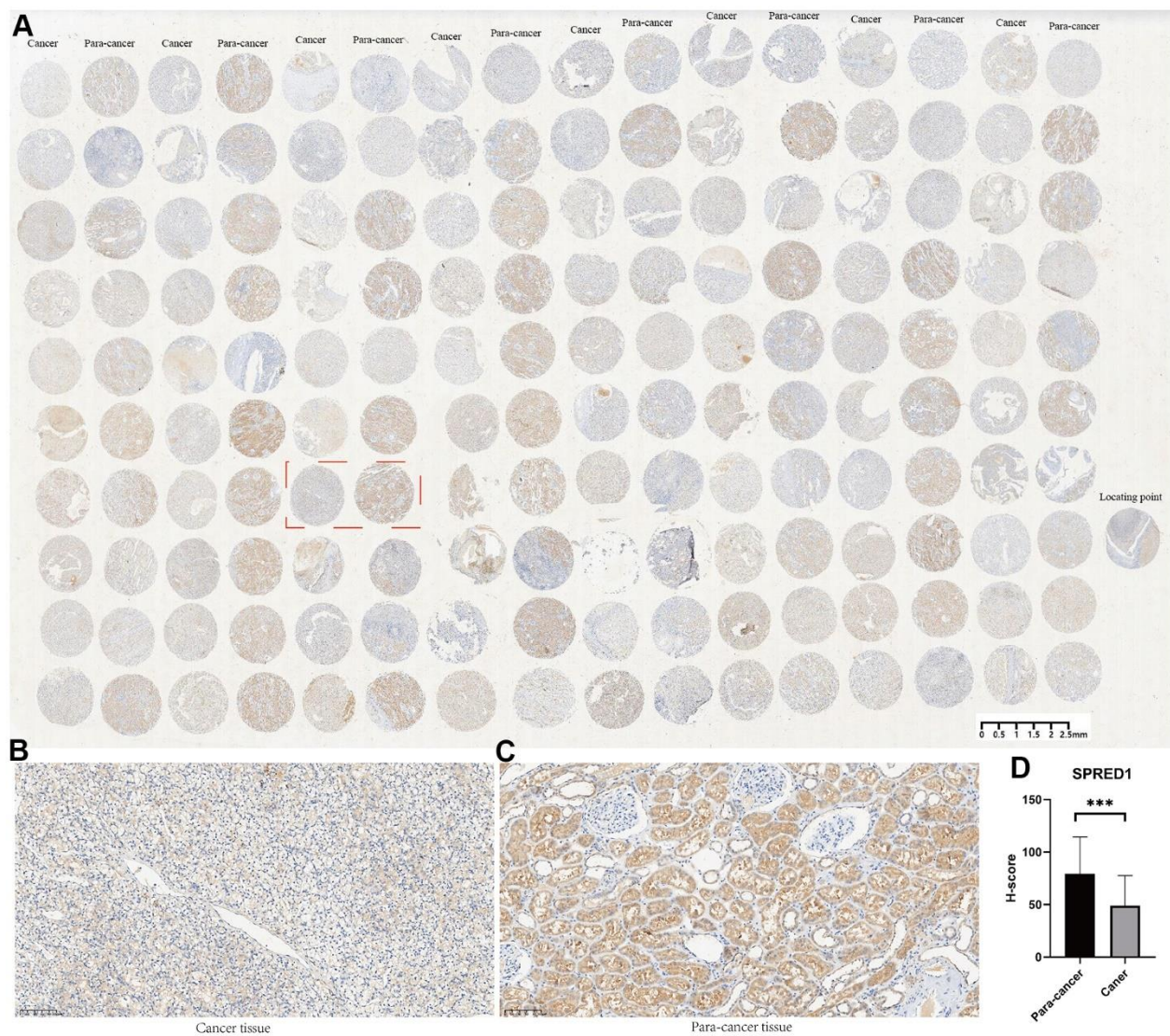
Supplementary Figure 4. The tissue microarray and immunohistochemistry (IHC) of SPRED1. (**A**) Immunohistochemical maps for all samples. (**B**) Immunohistochemical maps of typical cancer samples. (**C**) Immunohistochemical maps of typical para-cancer samples. (**D**) Immunohistochemical statistical analysis results.
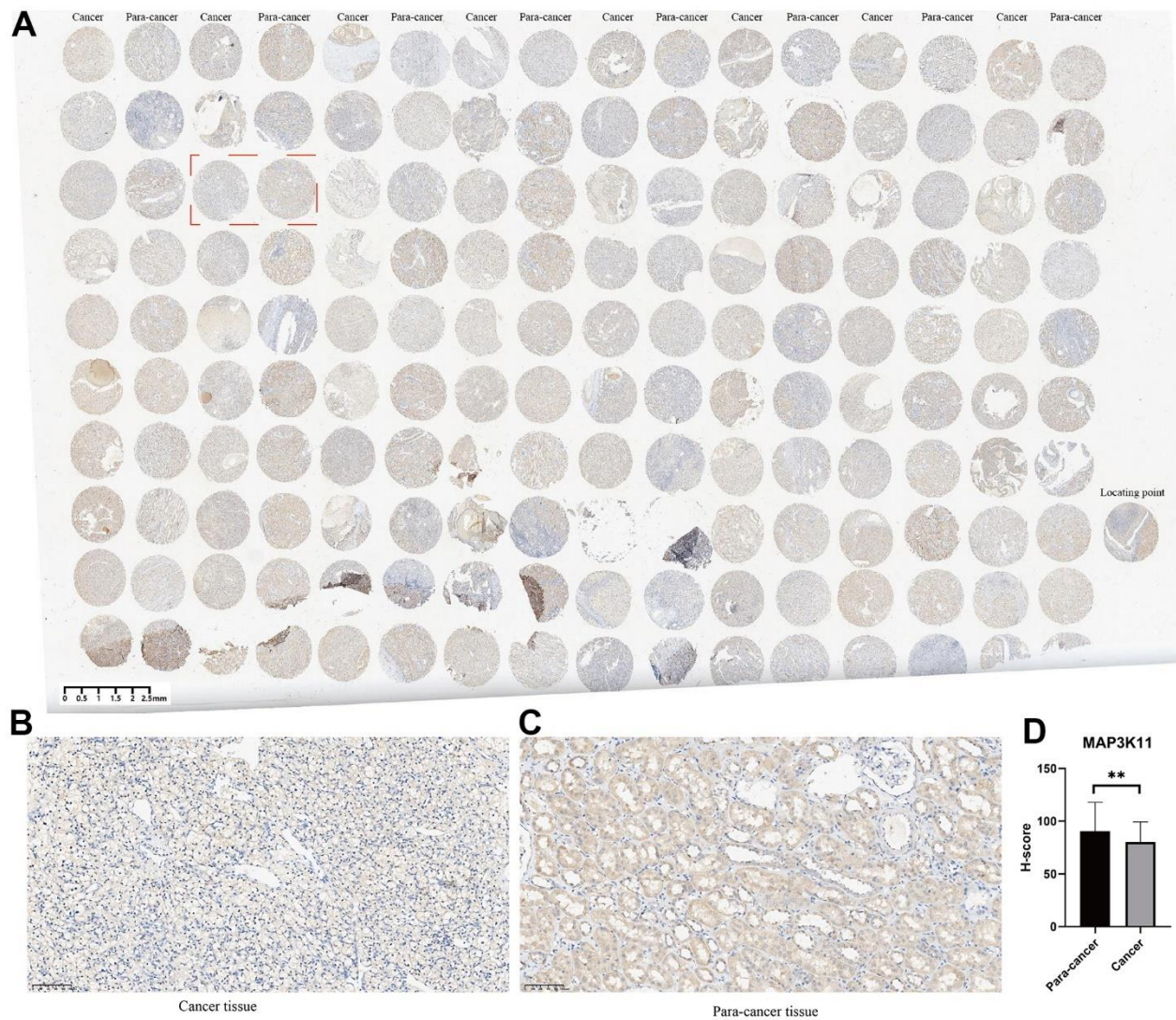
Supplementary Figure 5. The tissue microarray and immunohistochemistry (IHC) of MAP3K11. (**A**) Immunohistochemical maps for all samples. (**B**) Immunohistochemical maps of typical cancer samples. (**C**) Immunohistochemical maps of typical para-cancer samples. (**D**) Immunohistochemical statistical analysis results.